Am J Physiol Lung Cell Mol Physiol 314: L256–L275, 2018.
First published October 26, 2017; doi:10.1152/ajplung.00096.2017.

RESEARCH ARTICLE | *Translational Physiology*

Endothelial HIF-2α contributes to severe pulmonary hypertension due to endothelial-to-mesenchymal transition

Haiyang Tang,[1]* Aleksandra Babicheva,[1]* Kimberly M. McDermott,[1] Yali Gu,[1] Ramon J. Ayon,[1] Shanshan Song,[1] Ziyi Wang,[1] Akash Gupta,[2] Tong Zhou,[3] Xutong Sun,[1] Swetaleena Dash,[1] Zilu Wang,[1] Angela Balistrieri,[1] Qiuyu Zheng,[6] Arlette G. Cordery,[1] Ankit A. Desai,[1,2] Franz Rischard,[1,3] Zain Khalpey,[1,5] Jian Wang,[1,6] Stephen M. Black,[1] Joe G. N. Garcia,[1,3] Ayako Makino,[1,4] and Jason X.-J. Yuan[1,3,4]

[1]*Division of Translational and Regenerative Medicine, College of Medicine, University of Arizona, Tucson, Arizona;* [2]*Division of Cardiology, College of Medicine, University of Arizona, Tucson, Arizona;* [3]*Division of Pulmonary, Allergy, Critical Care, and Sleep Medicine, Department of Medicine, College of Medicine, University of Arizona, Tucson, Arizona;* [4]*Department of Physiology, College of Medicine, University of Arizona, Tucson, Arizona;* [5]*Department of Surgery, College of Medicine, University of Arizona, Tucson, Arizona; and* [6]*State Key Laboratory of Respiratory Disease, Guangzhou Institute of Respiratory Disease, The First Affiliated Hospital of Guangzhou Medicine University, Guangzhou, China*

Submitted 1 March 2017; accepted in final form 18 October 2017

Tang H, Babicheva A, McDermott KM, Gu Y, Ayon RJ, Song S, Wang Z, Gupta A, Zhou T, Sun X, Dash S, Wang Z, Balistrieri A, Zheng Q, Cordery AG, Desai AA, Rischard F, Khalpey Z, Wang J, Black SM, Garcia JG, Makino A, Yuan JX. Endothelial HIF-2α contributes to severe pulmonary hypertension due to endothelial-to-mesenchymal transition. *Am J Physiol Lung Cell Mol Physiol* 314: L256–L275, 2018. First published October 26, 2017; doi:10.1152/ajplung.00096.2017.—Pulmonary vascular remodeling characterized by concentric wall thickening and intraluminal obliteration is a major contributor to the elevated pulmonary vascular resistance in patients with idiopathic pulmonary arterial hypertension (IPAH). Here we report that increased hypoxia-inducible factor 2α (HIF-2α) in lung vascular endothelial cells (LVECs) under normoxic conditions is involved in the development of pulmonary hypertension (PH) by inducing endothelial-to-mesenchymal transition (EndMT), which subsequently results in vascular remodeling and occlusive lesions. We observed significant EndMT and markedly increased expression of SNAI, an inducer of EndMT, in LVECs from patients with IPAH and animals with experimental PH compared with normal controls. LVECs isolated from IPAH patients had a higher level of HIF-2α than that from normal subjects, whereas HIF-1α was upregulated in pulmonary arterial smooth muscle cells (PASMCs) from IPAH patients. The increased HIF-2α level, due to downregulated prolyl hydroxylase domain protein 2 (PHD2), a prolyl hydroxylase that promotes HIF-2α degradation, was involved in enhanced EndMT and upregulated SNAI1/2 in LVECs from patients with IPAH. Moreover, knockdown of HIF-2α (but not HIF-1α) with siRNA decreases both SNAI1 and SNAI2 expression in IPAH-LVECs. Mice with endothelial cell (EC)-specific knockout (KO) of the PHD2 gene, *egln1* (egln1$^{EC-/-}$), developed severe PH under normoxic conditions, whereas Snai1/2 and EndMT were increased in LVECs of egln1$^{EC-/-}$ mice. EC-specific KO of the HIF-2α gene, *hif2a*, prevented mice from developing hypoxia-induced PH, whereas EC-specific deletion of the HIF-1α gene, *hif1a*, or smooth muscle cell (SMC)-specific deletion of *hif2a*, negligibly affected the development of PH. Also, exposure to hypoxia for 48–72 h increased protein level of HIF-1α in normal human PASMCs and HIF-2α in normal human LVECs. These data indicate that increased HIF-2α in LVECs plays a pathogenic role in the development of severe PH by upregulating SNAI1/2, inducing EndMT, and causing obliterative pulmonary vascular lesions and vascular remodeling.

endothelial cell; intimal lesion; prolyl hydroxylase domain-containing protein; pulmonary arterial hypertension

INTRODUCTION

Idiopathic pulmonary arterial hypertension (IPAH) is a life-threatening disease with a 5-yr survival rate from the time of diagnosis of 68% (24). Sustained pulmonary vasoconstriction, excessive pulmonary vascular remodeling, in situ distal arterial thrombosis, and increased pulmonary vascular wall stiffness result in the increase of pulmonary vascular resistance (PVR) and pulmonary arterial pressure (PAP) in patients with idiopathic, heritable, and associated pulmonary arterial hypertension (PAH). Progressive pulmonary vascular remodeling, characterized by concentric pulmonary arterial wall thickening and obliterative intimal lesions, is one of the major causes for the elevation of PVR and PAP in almost all patients with IPAH (33, 59). Although lung vascular endothelial cell (LVEC) proliferation has been implicated in occlusive intimal lesions and plexiform lesions in small pulmonary arteries of patients with IPAH, the precise mechanism is not fully understood (59, 63).

Pathological studies indicate that the cell types found in the intraluminal occlusions contain cell markers of mesenchymal cells and smooth muscle cells (SMCs), while cell markers of endothelial cells (ECs) are not prominent (83). Endothelial-to-mesenchymal transition (EndMT) results in ECs obtaining markers of mesenchymal cells and SMCs, while concurrently losing EC markers (26). EndMT has recently been linked to the formation of obliterative vascular lesions in PAH (28, 30, 42, 55, 60). EndMT results in increased migratory capacity in

* H. Tang and A. Babicheva contributed equally to this study.

Address for reprint requests and other correspondence: J. Yuan, Div. of Translational and Regenerative Medicine, Dept. of Medicine, Univ. of Arizona, 1295 N. Martin Ave., PO Box 210202, Tucson, AZ 85721-0202 (e-mail: jasonyuan@email.arizona.edu).

1040-0605/18 Copyright © 2018 the American Physiological Society

Downloaded from journals.physiology.org/journal/ajplung at Midwestern Univ Lib (132.174.254.157) on December 20, 2022.

LVECs and may also play an important role in converting slowly proliferating LVECs to a highly proliferative cell type (e.g., myofibroblasts) contributing to the formation and progression of occlusive intimal lesions in patients with IPAH and animals with severe pulmonary hypertension (PH). In this study, we aimed at investigating the signaling pathways involved in EndMT in LVECs from patients with IPAH and animals with severe PH.

Hypoxia-inducible factor (HIF) is a family of transcription factors including three members: HIF-1, HIF-2, and HIF-3 (64). Although HIF-1α and HIF-2α proteins have similar functional domains and target expression of both overlapping and divergent genes, they may serve different functions in vascular morphogenesis and systemic hypoxic response (8, 9, 21, 31, 66, 85). Prolyl hydroxylase domain proteins (PHDs) hydroxylate conserved proline residues within HIF (5). Hydroxylation of HIF facilitates the binding of von Hippel-Lindau protein (VHL) to HIF, turning HIF into a substrate for E3 ubiquitin ligase and directs HIF polyubiquitylation and proteasomal degradation (5). We (27) and other investigators (22, 36, 78) have recently reported that endothelial-specific knockout (KO) of the PHD2 gene, *egln1*, results in spontaneous PH under normoxic conditions due to severe pulmonary vascular remodeling including obliterative pulmonary vascular lesions. Additionally, in response to low O_2, HIF-α subunits (e.g., HIF-1α, HIF-2α) have been shown to upregulate expression of members of the SNAI family of zinc-finger transcription factors, which are known inducers of EndMT (45, 81). In this study, we investigate the pathogenic roles of the PHD2/HIF-1/2α/SNAI signaling cascade and EndMT in the development and progression of PAH.

METHODS

Experimental animals and pulmonary hypertension models. All animal experiments were approved by the University of Arizona Animal Care and Use Committee and were performed according to the university guidelines that comply with national and international regulations. In the rodent models of PH, male C57BL/6J mice from Jackson Laboratories and Sprague-Dawley (SD) rats from Charles River Laboratories were utilized. Mice were exposed to room air (normoxia) or 10% O_2 (hypoxia) for 3–5 wk as previously described (72). After chronic exposure to normobaric hypoxia, mice were anesthetized with ketamine/xylazine before hemodynamic measurements or organ procurement for ex vivo experimentation. For monocrotaline (MCT)-mediated PH model, MCT is dissolved in 0.5 N HCl to 200 mg/ml, neutralized to pH 7.4 with 0.5 N NaOH, and then diluted with sterile water to 60 mg/ml. One dose of MCT (60 mg/kg body weight) was subcutaneously injected in rats. Control rats were injected with the equivalent volume of the dissolvent solution according to their weights. Food and water were provided ad libitum, and the rats were checked once per day. Phenotypic characterization studies were performed at either 2- or 4-wk time points after MCT injection.

Generation of KO mice. Cre-Lox technology was used to generate EC- or SMC-specific KO mouse lines according to the methods previously described (27, 72). The *egln1* floxed mice were crossed with *Tie2-Cre* mice for more than two generations to create *Tie2-Cre*$^{+}$*/egln1*$^{flox/flox}$ mice, referred to as EC-specific *egln1* KO mice (*egln1*$^{EC-/-}$). For the inducible and EC-specific KO mice, *hif1a* floxed mice and *hif2a* floxed mice were crossed with *Tie2-CreER*^{T2} mice to create *Tie2-CreER*$^{T2+}$*/hif1a*$^{flox/flox}$ mice or *Tie2-CreER*$^{T2+}$*/hif2a*$^{flox/flox}$ mice, referred to as inducible EC-specific *hif1α* KO mice (*hif1a*$^{EC-/-}$) and inducible EC-specific *hif2α* KO mice (*hif2a*$^{EC-/-}$), respectively. In these mouse strains, a tamoxifen-inducible Cre recombinase is under the control of the *tie2* promoter. The tamoxifen administration to induce gene KO was made as previously described (72). Mice were allowed to recover for 2 wk following the tamoxifen administration regimen before subsequent experimental manipulation.

Hemodynamic measurements in animals. Rats or mice were weighed before the experiment and once a week during the experiment. Right ventricular pressure (RVP), right ventricular systolic pressure (RVSP), and the Fulton index as a parameter of RV hypertrophy (RVH) were measured as previously described (73). For morphometric analysis, the lung tissues were fixed, embedded, and sectioned. Slides were stained with hematoxylin and eosin and used to determine and quantitate pulmonary arterial wall thickness as previously described (73).

Lung angiography. Rats were anesthetized with a simultaneous intraperitoneal injection of ketamine/xylazine cocktail and heparin (20 mg/kg body wt). Rats were examined for lack of tactile response to a footpad pinch to confirm proper sedation. Microfil polymer was mixed and injected into the beating RV, allowing the normal outflow of the right heart and the apparatus (NE-300, Pump Systems) to pump the Microfil into the arteries of the lung. After 45 min at room temperature, the heart and lungs were removed into a glass scintillation vial filled with 1X PBS. The tissues were then completely dehydrated (1 h/concentration) by ethanol using the following concentrations in the order of 50, 70, 80, 95, and 100% (2 times for 100%). After dehydration, the tissue-containing vial was filled with Methyl Salicylate (Sigma-Aldrich) and gently shaken overnight at room temperature. The lungs were then photographed with a microscope camera, and the ImageJ program (National Institutes of Health) was used to measure the number of branches—the number of junctions along the whole length of the pulmonary arterial tree in the lungs.

Isolated perfused/ventilated mouse lung experiment. The PAP was measured using the isolated perfused/ventilated mouse lung system as described previously (84). Briefly, mice were anesthetized and ventilated with a gas mixture of 21% O_2-5% CO_2 in N_2 via a rodent ventilator (minivent type 845; Harvard Apparatus). The pulmonary circulation was maintained in a closed circuit via a peristaltic pump (ISM 834; Isomatec). After basal PAP was stabilized for 40–60 min, the experiments were performed.

Human lung tissues and human EC culture. Approval for the use of human lung tissues and cells was granted by the University of Arizona Institutional Review Board. Human samples used in this study were derived from seven donor lung explants not suitable for lung transplantation and six idiopathic PAH (IPAH) patients. LVECs were obtained from Lonza or provided by the Pulmonary Hypertension Breakthrough Initiative. The demographic information is listed in

Table 1. *Demographic information of human subjects from whom LVECs are isolated for the study*

Subjects	Sex	Age	Race	Type of Cells
Failed donor-1	Male	25	White	Type II
Failed donor-2	Female	49	White	Type II
Failed donor-3	Female	46	Black	Type II
Failed donor-4	Female	49	White	EC-M
Failed donor-5	Male	51	White	EC-M
Failed donor-6	Female	55	White	EC-M
Failed donor-7	Male	49	White	EC-M
IPAH patient-1	Male	51	White	Type II
IPAH patient-2	Female	32	White	Type II
IPAH patient-3	Male	51	White	EC-M
IPAH patient-4	Male	16	White	EC-M
IPAH patient-5	Female	16	White	EC-M
IPAH patient-6	Female	22	White	EC-M

Based on the Pulmonary Hypertension Breakthrough Initiative definition, Type II denotes microvascular endothelial cell; EC-M denotes pulmonary arterial endothelial cell. LVECs, lung vascular endothelial cells; IPAH, idiopathic pulmonary arterial hypertension.

Downloaded from journals.physiology.org/journal/ajplung at Midwestern Univ Lib (132.174.254.157) on December 20, 2022.

Table 1. Cell line authentication has been carried with fluorescence-activated cell sorting (FACS) and immunocytochemistry (ICC) with CD31 (FACS), von Willebrand factor (vWF), and vascular endothelial cadherin (VE-cadherin) (ICC). The percentage of positive cells that exhibit CD31, vWF, and VE-cadherin signal was over 90% in human LVEC cultures. LVECs from normal controls and IPAH patients were cultured in flasks precoated with 0.1% gelatin in EBM-2 medium (Cat. No., CC-3156 Lonza) supplemented with EGM-2 MV Bullet Kit (Cat. No. 4147, Lonza) in a humidified 95% air-5% CO_2 incubator at 37°C. Human LVECs were used between passages four and nine for the experiments. In some experiments, cells were treated with transforming growth factor-β1 (TGF-β1) (10 ng/ml) for 7 days followed by cell collection and experimentation. TGF-β1 was reconstituted at 20 μg/ml in sterile 4 mM HCl containing 1 mg/ml bovine serum albumin (BSA) and then diluted with sterile water to 10 μg/ml. Vehicle group was treated with 4 mM HCl containing 1 mg/ml BSA. The medium was changed every other day. Cells were harvested for either RNA or protein isolation. For immunocytochemistry and proliferation assay, cells were grown on 12-mm-diameter coverslips followed by cell fixation and staining. Roxadustat (FG-4592) (Sigma-Aldrich) was used for pharmacological inhibition of PHD activity in vitro. FG-4592 was dissolved in 0.01% DMSO. Normal LVECs were treated with FG-4592 (100 μM) or vehicle (0.01% DMSO) for 4 h. Control siRNA (Cat. No. sc-37007, Santa Cruz Biotechnology), HIF-1α siRNA (Cat. No. sc-35561, Santa Cruz Biotechnology), or HIF-2α siRNA (Cat. No. c-35316, Santa Cruz Biotechnology) at the concentration of 60 pM were used with Lipofectamine RNAiMAX (Cat. No. 13778075, Invitrogen) for transfection in IPAH cells for 4–6 h. Cells were harvested for protein isolation 48 h after transfection. For hypoxia treatment experiments normal cells were exposed to hypoxia (3% O_2) in a humidified incubator at 37°C for 48–72 h.

Human smooth muscle cell culture. Approval for the use of human lung tissues and cells was granted by the UA Institutional Review Board. PASMC samples utilized in this study were derived from four donor lung explants not suitable for lung transplantation and 4 IPAH patients. Pulmonary arterial smooth muscle cells (PASMCs) were obtained from Lonza or provided by Cleveland Clinic. The demographic information of human PASMCs is listed in Table 2. Smooth muscle cell line authentication has been carried with α-smooth muscle actin (α-SMA) (FACs and ICC), SM22α (ICC), and smooth muscle myosin heavy chain (ICC). The percentage of positive cells that exhibit α-SMA, SM22α, and smooth muscle myosin heavy chain signal was over 95% in human PASMC cultures. PASMCs were cultured in 100-mm dishes in SmGM-2 medium (Cat. No. CC-3181, Lonza,) supplemented with SmGM-2 SingleQuot Bullet Kit (Cat. No. 4149, Lonza) in a humidified 95% air, 5% CO_2 incubator at 37°C. The medium was changed every other day. Cells were allowed to grow to 80–90% confluence and harvested for protein isolation. For hypoxia treatment, experiments normal cells were exposed to hypoxia (3% O_2) in a humidified incubator at 37°C for 48–72 h.

Isolation and preparation of mouse lung pulmonary vascular ECs. Mouse lung vascular ECs were isolated based on a method previously described (17). Briefly, the lungs were quickly dissected from the anesthetized mouse, and lung tissues were minced and incubated for 1 h at 37°C with M199 containing 1 mg/ml collagenase II and 0.6 U/ml dispase II. The digested tissues and cells were filtered using sterile 40-μm nylon mesh and washed in M199 containing 2% fetal calf serum. The filtered cell suspension was then incubated with Dynabeads (Invitrogen) at 4°C for 1 h, and beads attached to ECs were then isolated or captured by Dynal magnet (Invitrogen). For EC isolation, beads were first coated with sheep anti-rat IgG and incubated with purified rat anti-mouse CD31 monoclonal antibody (1 μg/ml) overnight at 4°C and then washed with a PBS solution containing 0.1% BSA and 2 mM EDTA. The purity of ECs in isolated cells from lungs was tested by DiI-acLDL uptake and *Bandeiraea simplicifolia* lectin-FITC (BS-l, Sigma-Aldrich) staining. Cultured human PASMCs were used as negative control. Mouse lung vascular ECs were seeded on a coverslip, cultured at 37°C, fixed, and stained as previously described (17). The percentage of positive cells that exhibit both acLDL and BS-l signal was over 93% in mouse lung vascular EC cultures.

Table 2. *Demographic information of human subjects from whom PASMCs are isolated for the study*

Subjects	Sex	Age	Race	Type of Cells
Failed donor-1	Female	56	White	PASMC
Failed donor-2	Male	57	White	PASMC
Failed donor-3	Male	35	Hispanic	PASMC
Failed donor-4	Female	51	Hispanic	PASMC
IPAH patient-1	Female	32	White	PASMC
IPAH patient-2	Male	41	White	PASMC
IPAH patient-3	Male	45	White	PASMC
IPAH patient-4	Female	57	White	PASMC

PASMC, pulmonary arterial smooth muscle cell.

5′-Ethynyl-2′-deoxyuridine cell proliferation assay. LVECs from normal subjects and IPAH patients were seeded on 12-mm-diameter coverslips at a density of 1×10^4. LVECs from both groups were treated with 10 μM 5′ethnyl-2′-deoxyuridine (EdU) (Life Technologies) 24 h at 37°C after the initial plating to monitor cell proliferation. The cells were fixed and permeabilized after 24 h of EdU incubation, followed by labeling and detection of newly synthesized DNA using the Click-iT EdU Alexa Fluor 594 imaging kit (Thermo Fisher Scientific). Hoechst 33342 (1:2,000) (Molecular Probes) was used to counterstain nuclear DNA. The coverslips were mounted on glass slides by using ProLong Diamond Antifade Mountant (Life Technologies). All reagents were prepared according to manufacturer's instructions. The stained cells were examined using a Zeiss AxioObserver.Z1 fluorescence microscope (Carl Zeiss Microscopy), and nuclear images were acquired using the Zen Pro 2012 imaging software (Carl Zeiss Microscopy). Six fields (~60–75 cells/field) on each coverslip were randomly selected to measure proliferation rate as a percentage of EdU incorporation.

Real-time RT-PCR analysis. Total RNA was isolated from lung tissues (50–100 μg) or primary cultured LVECs by using QIAzol reagent (Qiagen). After homogenization, the tissue or cell samples were processed according to QIAzol reagent instructions. To eliminate residual contaminating genomic DNA, the RNA preparation was further treated with RNase-free DNase (Thermo Scientific) (1 U/1 μg RNA) for 30 min at 37°C. The RNA was dissolved in 20–50 μl RNase-free water depending on the quantity of the precipitation and stored at −80°C. Determination of RNA concentration and purity was performed by optical density (OD) measurement (ratio of OD at 260 nm to OD at 280 nm is greater than 1.7) using a Nano-Drop spectrophotometer (Thermo Scientific). Integrity and quality of RNA were evaluated by 1.5% agarose gel electrophoresis.

One microgram of RNA was converted to first-strand cDNA by using a High Capacity cDNA Reverse Transcription (RT) Kit with random primers (Applied Biosystems). The cDNA samples were amplified with mRNA-specific primers in a Thermal Cycler (Bio-Rad). PCR primers were purchased from Integrated DNA Technologies. An invariant mRNA of GAPDH was used as an internal control to normalize the PCR products. The PCR products were electrophoresed through 1.5% agarose gel, and amplified cDNA bands were visualized by Photo Imager (VWR). The real-time PCR amplification was conducted with iTaq Universal SYBR Green Supermix (Bio-Rad) by using mRNA-specific primers and completed by 100 ng of synthesized cDNA in a CFX96 real-time PCR detection system (Bio-Rad) in triplicate. Melting curve analysis was performed to evaluate the specificity of primers. Oligonucleotide primers used in this study are listed in Table 3. GAPDH as a reference gene was also used to normalize C_t values. A no template control was included in each PCR run to control for contamination. We used the $2^{-\Delta\Delta Ct}$ method to calculate relative quantification of mRNA expression. $\Delta\Delta C_t$ formula

Downloaded from journals.physiology.org/journal/ajplung at Midwestern Univ Lib (132.174.254.157) on December 20, 2022.

Table 3. *Oligonucleotide primers used for PCR in this study*

Gene Names (GenBank accession no.)	Predicted Size, bp	Sense	Antisense	Location, Nucleotides
Human				
SNAI1 (NM_005985.3)	150	5′-GTTCTTCTGCGCTACTGCTG-3′	5′-TTAGGTCTCAAATGGAAGGTCGT-3′	33–182
SNAI2 (NM_003068.4)	200	5′-GACACATTAGAACTCACACGGG-3′	5′-GACCGACGACACATCGTGTG-3′	780–979
PECAM1 (NM_000442.4)	130	5′-TTGAGACCAGCCTGATGAAACCCT-3′	5′-ATAGCGAACTTGGGTCCTTTGCCT-3′	3318–3447
CDH5 (NM_001795.3)	260	5′-TGTGGGCTCTCTGTTTGTTG-3′	5′-CTTTGTCTCGGGTCCAGTAA-3′	999–1258
ACTA2 (NM_001141945.2)	186	5′-TCCCTGAACACCACCCAGTG-3′	5′-CACTGTTACCGAGACCCGAG-3′	439–624
S100A4 (NM_002961.2)	140	5′-AGTCAGAACTAAAGGAGCTGC-3′	5′-CTGAAGGTTCTCATGACACAG-3′	161–300
FN1 (NM_212482.2)	172	5′-AACAAACACTAATGTTAATTGCCCA-3′	5′-CGTCTGGGTCGAATCTCAAGA-3′	7619–7790
MKI67 (NM_001145966.1)	109	5′-TGGGTCTGTTATTGATGAGCC-3′	5′-CAGAAGTCTTACCTTCCTTCAGT-3′	411–519
PHD1 (or *Egln2*) (NM_053046.3)	194	5′-AGCCCCTAAGTCAGGCTCTC-3′	5′-GGTGTCGGTGGAGATGGTGA-3′	467–660
PHD2 (or *Egln1*) (NM_022051.2)	147	5′-GGGACATTCATTGCCTCACTCTC-3′	5′-CTAACCCGTGTATTGTCGTTCG-3′	120–266
PHD3 (or *Egln3*) (NM_001308103.1)	86	5′-GGCATCACGGAAGCCTTAACA-3′	5′-ACAAGAATTAGGTCCCGACAACC-3′	917–1002
HIF-1α (NM_001243084.1)	98	5′-CAAGAACCTACTGCTAATGCCACC-3′	5′-GTAGAGGTAGAGGATGGGTGTATG-3′	2123–2220
HIF-2α (or *EPAS-1*) (NM_001430.4)	196	5′-TCTGAAAACGAGTCCGAAGCC-3′	5′-TGAAGTGAGTAGGGACGCTGG-3′	733–928
GAPDH (NM_001289746.1)	144	5′-GCACCGTCAAGGCTGAGAAC-3′	5′-TGACCGCAGAAGTGGTGGTA-3′	2574–2717
Rat				
Snai1 (NM_053805.1)	155	5′-AGAGTTGTCTACCGACCTTGC-3′	5′-CGCACACACCTCAAGTGGAAG-3′	19–173
Snai2 (NM_013035.1)	192	5′-CACACACAGTGATCATTTCTCCA-3′	5′-TAGAAACCCCGCACATTCGG-3′	71–262
Pecam1 (NM_031591.1)	154	5′-TCTCCATCCTGTCGGGTAACG-3′	5′-CTTTGGCACTTACTGTGGGTTC-3′	1676–1829
Cdh5 (NM_001107407.1)	107	5′-AACAACCACGACAATACCGC-3′	5′-TAGAGGCTGTTACCCTACGG-3′	1619–1725
Ctnnd1 (NM_001107740.1)	132	5′-GAGCACCCTTGATGCAGAAGA-3′	5′-AGCGACCTGATAACACGGTT-3′	3147–3278
Acta2 (NM_031004.2)	152	5′-GGAGATGGCGTGACTCACAA-3′	5′-AAGCACTGATGACGACTCGC-3′	529–680
Vim (NM_031140.1)	113	5′-*GCTGCGAGAAAAATTGCAGG*-3′	5′-ACCGTGCAGAACTGGAACTT-3′	632–744
Mki67 (NM_001271366.1)	199	5′-CTGGTCACCATCAAGCGGAG-3′	5′-TCAGTTTCTCGTTCTCCGTTATAA-3′	402–600
Gapdh (NM_017008.4)	156	5′-GCAAGGATACTGAGAGCAAGAG-3′	5′-TATTTCAAGCGACGTGGGAG-3′	1121–1276
Mouse				
Snai1 (NM_011427.3)	167	5′-TTGTGTCTGCACGACCTGTGGAAA-3′	5′-TGGGTGAGCCTACACTTCT-3′	632–798
Snai2 (NM_011415.2)	164	5′-CACATTCGAACCCACACATTGCCT-3′	5′-TCTGTCTAGTTTGGACTCCCGTGT-3′	647–810
Pecam1 (NM_001032378.2)	158	5′-AAGCCAACAGCCATTACGGT-3′	5′-GTGGTTCTCTTGCCTTCCGA-3′	2169–2326
Cdh5 (NM_009868.4)	115	5′-GCTCACGGACAAGATCAGCTC-3′	5′-AAGGGGTCTATCTGTGGGGG-3′	96–210
Acta2 (NM_007392.3)	140	5′-CGTGGCTATTCCTTCGTGAC-3′	5′-CCTCTTCTCGATGCTTGCG-3′	699–838
S100A4 (NM_011311.2)	193	5′-AGCACTTCCTCTCTCTTGGTC-3′	5′-GGACCCCTTTTCCTGTCTACT-3′	15–207
Phd2 (or *Egln1*) (NM_053207.2)	268	5′-AGAAGGCAAAGCCCAGTTTG-3′	5′-CGTCATGGGTGCAGTGGATG-3′	1172–1439
Gapdh (NM_001289726.1)	151	5′-GTGTCCGTCGTGGATCTGA-3′	5′-GAGGACGCTGAAGTTGTCGTT-3′	802–952

is as follows: $\Delta\Delta C_t = \Delta C_{t1} - \Delta C_{t2}$, where $\Delta C_{t1} = C_t$ of the mRNA target (experimental sample) – C_t of the mRNA reference gene (experimental sample) and $\Delta C_{t2} = C_t$ of mRNA target (control sample) – C_t of the mRNA reference gene (control sample).

Western blot analysis. Lysed lung tissues or cells were sonicated and centrifuged at 12,000 rpm for 15 min at 4°C. The supernatants were collected, and protein concentration was determined by BCA protein assay reagent (Thermo Fisher Scientific) by using BSA as a standard. Cell lysates with equal quantities of protein (50 mg) were mixed and boiled in 6 × SDS sample buffer (Boston BioProducts). Protein suspensions were electrophoretically separated on an 8% acrylamide gel, and protein bands were transferred to nitrocellulose membranes by electroblot in a Mini Trans-Blot cell transfer apparatus (Bio-Rad) under conditions recommended by the manufacturer. After 1 h of incubation in blocking buffer (5% nonfat milk powder in 1 × TBS containing 0.1% Tween 20) for 1 h at room temperature, the membranes were then incubated with anti-Phd2 (Cat. No. 4835, Cell Signaling), anti-Hif1α (Cat. No. 610958, BD Transduction Laboratories), anti-Hif-2α (Cat. No. NB100-122, Novus), anti-Snai1 (Cat. No. 3879, Cell Signaling), anti-Snai2 (Cat. No. 9585, Cell Signaling), and anti-β-actin (Cat. No. sc-47778, Santa Cruz Biotechnology) overnight at 4°C. Finally, the membranes were washed and exposed to anti-rabbit and anti-mouse horseradish peroxidase-conjugated IgG for 60 min at room temperature. The bound antibody was detected with an enhanced chemiluminescence detection system (Thermo Fisher Scientific). Band intensity was normalized to β-actin controls and is expressed in arbitrary units.

Immunofluorescence. Human LVECs were grown on 12-mm-diameter coverslips and treated with TGF-β1 as described above. Cells were fixed with 4% paraformaldehyde (Cat. No. 15714, EM Sciences) at 37°C for 10 min or with 100% methanol for 10 min at −20°C. For antigen retrieval, cells grown on coverslips were incubated at room temperature (22–24°C) with 0.1% TritonX-100 in PBS for 5 min, followed by incubation with 0.05% SDS. Murine and rat paraffin-embedded tissue sections were sectioned and deparaffinized in xylene followed by isopropanol dilutions. Antigen retrieval was performed in 10 mM Citrate Buffer, pH 6. Cell and tissue sections were blocked with antibody dilution buffer (Cat. No. ADB250, Ventana Medical Systems) for 1 h at room temperature. Cells were stained with antibodies against SNAI1 (Cat. No. ab53519, Abcam), SNAI2 (Cat. No. 9585, Cell Signaling), platelet/EC adhesion molecule 1 (PECAM1) (Cat. No. ab645593, Abcam), vimentin (VIM) (Cat. No. 5741, Cell Signaling), cadherin 5 (CDH5) (Cat. No. ab33168Abcam), SM α-actin (ACTA2) (Cat. No. ab7817, Abcam), transgelin (TAGLN) (Cat. No. ab14106, Abcam), S100A4 (Cat. No. ABF32, Millipore). Antibodies were diluted in antibody dilution buffer and stained overnight at 4°C. Primary antibodies were detected using AlexaFluor conjugated isotype-specific secondary antibodies (1:1,000; Invitrogen) diluted in antibody dilution buffer to stain for 1 h at room temperature. Nuclei were stained with Hoechst (1:1000; Cat. No. H3570, Invitrogen) diluted in PBS for 10 min. Coverslips were mounted on slides in Prolong Gold (Cat. No. P36934, Invitrogen).

Immunohistochemistry experiment. Human and murine paraffin-embedded tissue sections used for the immunohistochemistry experiments were sectioned and deparaffinized in xylene followed by isopropanol dilutions. Antigen retrieval was performed with 10 mM sodium citrate buffer (10 mM sodium citrate, 0.05% Tween 20, pH 6.0) for staining with an antibody recognizing HIF-2α (Cat. No. ab73895, Abcam). A goat anti-rabbit secondary antibody conjugated to peroxidase (Cat. No. ab6721, Abcam) was incubated on the tissue

Downloaded from journals.physiology.org/journal/ajplung at Midwestern Univ Lib (132.174.254.157) on December 20, 2022.

for 60 min at room temperature (22–24°C), followed by detection with the peroxidase substrate 3,3′-diaminobenzidine (Cat. No. K3467, Dako). The tissues were counterstained with hematoxylin 1 (Cat. No. 7221, Thermo Scientific). Slides were mounted with Faramount Aqueous Mounting Media (Cat. No. S3025, Dako).

Immunofluorescence imaging and analysis. Fluorescently stained cells and tissue sections were imaged with a Leica TCS SP5 II laser scanning confocal microscope with a ×20 (0.7NA PL Apo; Leica Microsystems) or ×63 objective (1.4NA PL Apo; Leica Microsystems). Z-stacks were acquired at a total thickness of 6.0 ± 0.5 μm. Z images were processed postacquisition to maximum projections by using the Leica LAS AF software. At least three images were obtained per sample. Mean fluorescence intensity was quantified in 10 regions of interest per image. Discontinuous adherens junctions were quantified from cells grown to confluence in vitro and imaged to detect antibodies recognizing adherens junction proteins (PECAM1 or CDH5). For each cell, the associated adherens junctions were imaged at ×63 and scored as either having smooth staining along the adherens junction (continuous) or as having at least one gap along the adherens junction (discontinuous).

Antibody validation. The antibodies we used in this study have all been validated by many investigators who conducted similar experiments. The anti-PHD2 antibody (Ab) (Cat. No. 4835, CST) was validated in Western blot experiments by using lung ECs isolated from wild-type (WT) and *Egln1*^{Tie2} mice (22). This antibody was also confirmed by WB experiments in human bone osteosarcoma epithelial cells transfected with control and PHD2 siRNA (40). The anti-HIF-1α antibody (Cat. No. 610958, BD Transduction Laboratories) was validated by WB experiments using human colon carcinoma cells transfected with or without HIF-1α siRNA under normoxic and hypoxic conditions (13). Additionally, this antibody was validated by WB experiments in WT human embryonic stem cells and two CRISPR-Cas9 HIF-1α-KO mutants (67). To determine hypoxia-induced increases in HIF-1α and HIF-2α protein levels, we used antibodies against HIF-1α (no. 610959) and HIF-2α (no. NB100-122) that were validated by WB analysis in human ECs treated with control and siRNA or shRNA (27). The antibody for HIF-2α (no. NB100-122) was also validated by Western blot experiments in human breast adenocarcinoma cells transfected with HIF-2α shRNA (48). The anti-SNAI1 antibody (Cat. No. 3879, Cell Signaling) was validated by Western blot experiments in human prostate cancer cells overexpressing *SNAI1* and by targeting knockdown of SNAI1 with shRNA (56). This antibody was validated by siRNA-meditated knockdown of SNAI in human mammary epithelial cells (87). Another anti-SNAI1 antibody (Cat. No. ab53519, Abcam) we used in this study was verified by using SNAI1 knockdown with shRNA in HEK-293 cells (86). The anti-SNAI2 antibody (Cat. No. 9585, Cell Signaling) was validated by Western blot experiments in breast cells isolated from WT and *snai2*-KO mice (14). The anti-VIM antibodies (Cat. No. 5741, Cell Signaling, and Cat. No. ab20346, Abcam) were validated in Western blot experiments showing that treatment with siRNA for VIM (for 72 h) significantly downregulated VIM, whereas treatment with control nontargeting siRNA had no significant effect on endogenous VIM expression (11). The anti-CDH5 antibody (Cat. No. ab33168, Abcam) was validated by the company's customers, and the vender guaranteed that this product worked in Western blot experiments in which siRNA targeting CDH5 significantly decreased the CDH5 expression level. The anti-ACTA2 antibody (Cat. No. ab7817, Abcam) was validated by Western blot experiments and immunocytochemical-staining indicating that untreated control cells showed no expression of smooth muscle α-actin (SMA) or ACTA2, whereas TGF-β1 stimulation strongly increased SMA/ACTA2 protein expression level (68). The polyclonal anti-AGLN antibody (cat. nos. ab14106 and ab10135, Abcam) was validated by Western blot, immunohistochemistry, and immunocytochemistry experiments in human, mouse, and rat tissues and cells. These experiments showed that stable depletion of SM22α or AGLN by specific shRNA achieved 57% knockdown of SM22α or AGLN in cells expressing AGLN-shRNA compared with cells expressing a control sense RNA hairpin (16, 54, 58, 74). The anti-S100A4 antibody (Cat. No. ABF32, Millipore) was validated by Western blot and immunocytochemistry experiments showing that the parental cells infected with the empty vector expressed very low level of S100A4, whereas S100A4-expressing cells established by retroviral infection expressed a much higher level of the fibroblast-specific protein 1 (S100A4) (43).

Statistics. The composite data are expressed as means ± SE. Statistical analysis was performed using paired or unpaired Student's *t*-test or ANOVA and post hoc tests (Student-Newman-Keuls) where appropriate. Differences were considered to be significant at $P < 0.05$.

RESULTS

EndMT markers and proliferation rate are significantly enhanced in LVECs from IPAH patients. EndMT is characterized by the loss of cell-cell adhesion and the conversion of the cell phenotype to that of a spindle-shaped cell. Molecular changes associated with EndMT include a decrease in EC markers, such as platelet/EC adhesion molecule 1 (PECAM1) or CD31 and VE-cadherin or CDH5, as well as increased expression of mesenchymal cell markers, such as the fibroblast markers VIM, fibronectin 1 (FN1), and calcium-binding protein S100A4, and the SMC markers, such as ACTA2 and TAGLN (26). Moreover, the SNAI zinc-finger family of transcription factors (SNAI1, SNAI2, and SNAI3, also known as SNAIL, SLUG, and SMUC, respectively) has also been shown to have increased expression that is important in the progression of EndMT (38). To investigate whether LVECs from patients with IPAH display phenotypic and molecular changes typical of EndMT, we compared the mRNA and protein expression levels of EndMT biomarkers in LVECs from normal subjects and patients with IPAH. As shown in Fig. 1, LVECs from IPAH patients exhibited significantly *1*) upregulated mRNA expression level of SNAI1 and SNAI2; *2*) downregulated mRNA expression of biomarkers of the endothelial lineage including platelet and EC adhesion molecule 1 (PECAM1, also known as CD-31) and vascular endothelial cadherin (CDH5); *3*) increased mRNA expression of biomarkers of SMC lineage including ACTA2; and *4*) increased mRNA expression of fibroblast-specific protein S100A4 (also known as FSP1) and FN1 (Fig. 1*A*) in comparison to normal LVEC. Furthermore, the immunocytochemistry experiments also showed that the protein expression of SNAI1 (EndMT marker) was significantly increased, the protein expression of PECAM1 (EC marker) was decreased, and the protein expression level of the SMC marker TAGLN (also known as SM22) was increased in IPAH-LVECs compared with normal LVECs (Fig. 1, *B* and *C*). Cells from early (4–6) and late (6–9) passages were used for experiments and showed similar results. These data indicate that IPAH-LVECs undergoes EndMT.

To determine if LVECs from patients with IPAH have a higher proliferative index, we compared EdU incorporation and expression of a proliferation marker (MKI67) in LVECs from normal subjects and patients with IPAH. EdU incorporation (Fig. 1, *D* and *E*, *left*), as well as cell number (Fig. 1*E*, *right*), in IPAH-LVECs cultured in 2% FBS-DMEM were significantly greater than in normal LVECs. The enhanced proliferation rate of IPAH-LVECs was also associated with a significantly upregulated mRNA expression level of *MKI67* (Fig. 1*F*). These data indicate that the enhanced EndMT

Downloaded from journals.physiology.org/journal/ajplung at Midwestern Univ Lib (132.174.254.157) on December 20, 2022.

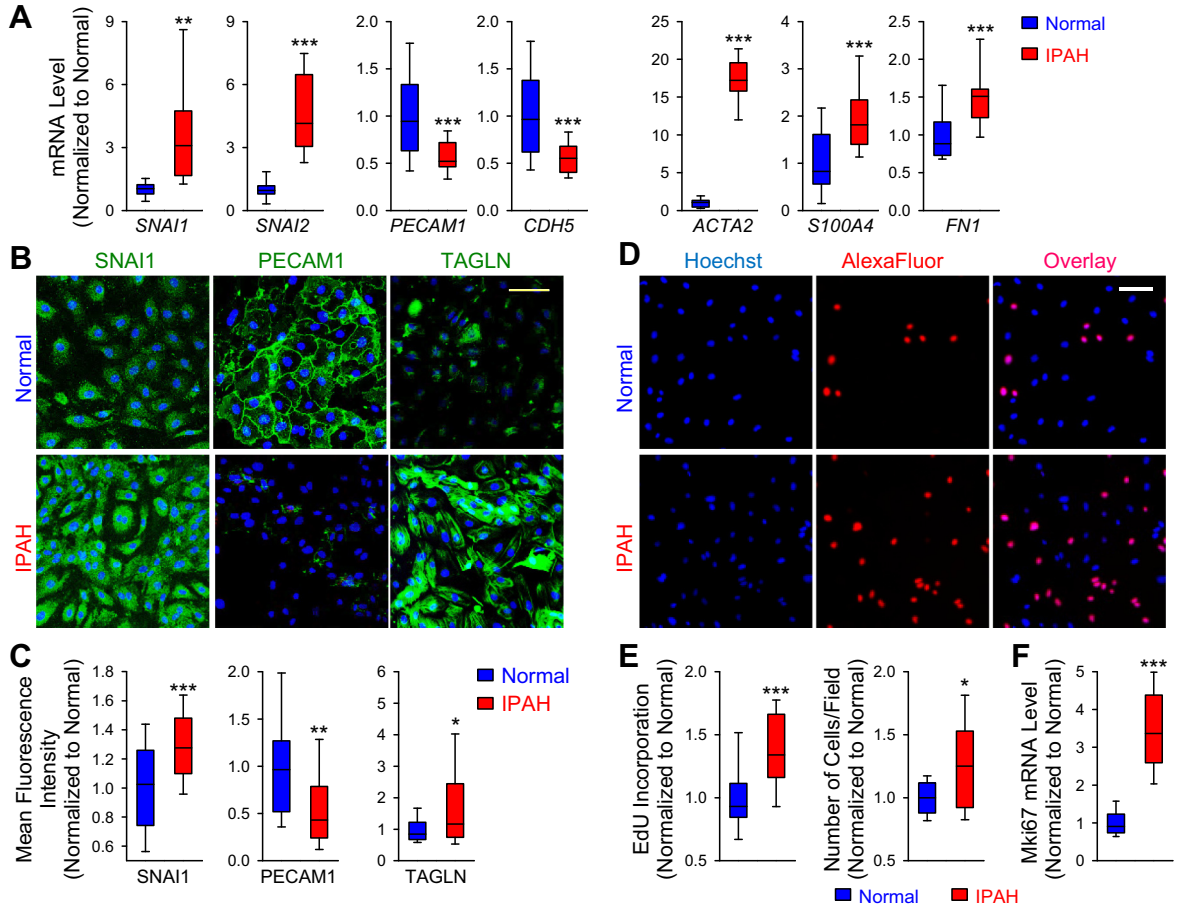

Fig. 1. Endothelial-to-mesenchymal transition (EndMT) and cell proliferation are enhanced in lung vascular endothelial cells (LVECs) isolated from patients with idiopathic pulmonary arterial hypertension (IPAH). *A*: real-time RT-PCR analysis of *SNAI1*, *SNAI2*, *PECAM1*, *CDH5*, *ACTA2*, *S100A4*, and *FN1* (normalized to *GAPDH* expression) in LVECs isolated from healthy subjects ($n = 7$) and IPAH patients ($n = 6$). *B*: representative images showing immunofluorescence in normal and IPAH-LVECs stained for SNAI1, PECAM1, and TAGLN. Nuclei counterstained with Hoechst. Scale bar, 100 μm. *C*: summarized data showing the mean fluorescence intensity for each antigen in normal and IPAH-LVECs ($n = 3$ per group; for each experiment, we analyzed three fields of view with 10 regions of interest per field of view). *D*: representative images showing nuclear staining (*left*, Hoechst, blue), 5′ethynyl-2′-deoxyuridine (EdU) staining (*middle*, AlexaFluor, red), and overlay images (*right*, overlay, purple) of normal and IPAH-LVECs. Scale bar, 100 μm. *E*: summarized data showing the percentage of cells with EdU incorporation (*left*) and the percentage of total cell number (*right*) in normal and IPAH-LVECs ($n = 3$ per group; for each experiment, we analyzed 3 fields of view with 6 regions of interest per field of view). *F*: real-time RT-PCR analysis of *MKI67* (normalized to *GAPDH* expression) in normal ($n = 7$) and IPAH ($n = 6$) LVECs. Values are median ± CI. $^*P < 0.05$; $^{**}P < 0.01$; $^{***}P < 0.001$ vs. normal.

observed in LVECs from IPAH patients was indeed associated with increased proliferation.

TGF-β1 induces EndMT in normal human LVECs to a level similarly seen in IPAH-LVECs. Transforming growth factor β (TGF-β) is a fibrotic factor that is known to induce EndMT in many cell types including LVECs (25, 46, 49, 61). To determine if TGF-β1 induces phenotypic changes of LVECs we compared the cell length of normal LVECs treated with vehicle or TGF-β1 (10 ng/ml) for 7 days and IPAHs cells. Our experiments revealed that the length of LVECs isolated from IPAH patients were distinctly larger or longer compared with groups treated with vehicle or TGF-β1 at *day 1* (Fig. 2*A*). At *day 7* of TGF-β1 treatment, LVECs exhibited significantly increased cell length compared with TGF-β1-treated cells at *day 1* and the cells treated with vehicle at *day 7* (Fig. 2*A*, *right*). The morphology of LVECs treated with TGF-β1 for 7 days changed from a cobblestone to spindle-shaped, fibroblast-like appearance similar to that observed in LVECs isolated from patients with IPAH. In normal LVECs, PECAM1 localizes to adherens junctions that form continuous cell-cell contacts. Immunofluorescence staining to visualize adherens junctions (using PECAM1 staining) revealed that normal LVECs formed continuous adherent junctions; however, LVECs from IPAH patients and the normal LVECs treated with TGF-β1 both exhibited a significant increase in discontinuous adherens junctions (Fig. 2*B*).

To examine if TGF-β1 induces EndMT in normal LVECs, we compared the mRNA and protein expression levels of EndMT biomarkers in LVECs from normal subjects to that of normal LVECs treated with TGF-β1 for 7 days. As shown in Fig. 2*C*, treatment of normal LVECs with TGF-β_1 significantly *1*) increased protein expression level of SNAI1, *2*) decreased protein expression of PECAM1, *3*) increased protein expression of VIM, and *4*) increased protein expression of TAGLN. Moreover, mRNA expression of EndMT-related transcription factors (*SNAI1* and *SNAI2*) and of mesenchymal (*ACTA2* and *FN1*) markers were upregulated while endothelial (*PECAM1* and *CDH5*) markers were downregulated (Fig. 2*D*). These

Downloaded from journals.physiology.org/journal/ajplung at Midwestern Univ Lib (132.174.254.157) on December 20, 2022.

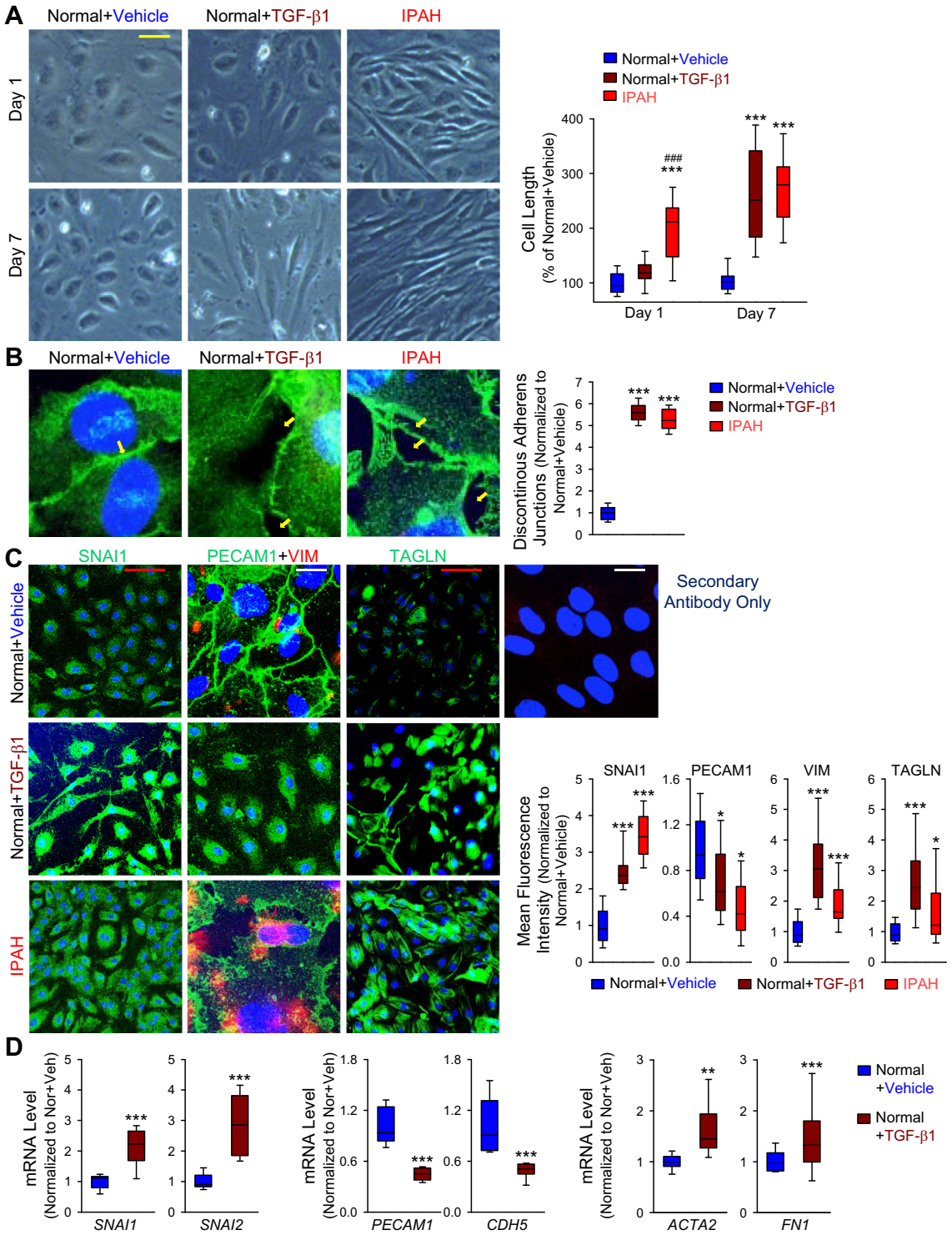

Fig. 2. Transforming growth factor-β1 (TGF-β1) induces EndMT in normal LVECs to a level similar observed in IPAH-LVECs. *A*: representative images (panels at *left*) and summarized data (panel at *right*) showing cell length in normal LVECs treated with vehicle or TGF-β1 (10 ng/ml) and IPAH-LVECs at *day 1* or day 7 (n = 3 per group). Scale bar, 30 μm. Values are median ± CI. ***$P < 0.001$ vs. vehicle; $^{###}P < 0.001$ vs. TGF-β1. *B*: representative images (panels at *left*) showing immunofluorescence in normal LVECs treated with vehicle or TGF-β1 (10 ng/ml) for 7 days and IPAH-LVECs stained for PECAM1 and summarized data (panel at *right*) showing the fraction of adherens junctions that are discontinuous with adjacent cells (n = 3 per group; for each experiment, we analyzed 3 fields of view with 10 regions of interest per field of view). Yellow arrows highlight the continuous and discontinuous adherens junctions. *C*: representative images (panels at *left*) and summarized data (panels at *right*) showing the mean fluorescence intensity in normal LVECs treated with vehicle or TGF-β1 (10 ng/ml) for 7 days and IPAH-LVECs stained for SNAI1, PECAM1, vimentin (VIM), and TAGLN (n = 3 per group; for each experiment, we analyzed 3 fields of view with 10 regions of interest per field of view). Cells stained with secondary antibody only were used as a negative control. Nuclei counterstained with Hoechst. Red scale bars, 100 μm; white scale bars, 20 μm. *D*: real-time RT-PCR analysis of *SNAI1*, *SNAI2*, *PECAM1*, *CDH5*, *ACTA2*, and *FN1* (normalized to *GAPDH* expression) in normal LVECs treated with vehicle or TGFβ1 (10 ng/ml) for 7 days (n = 3 per group). Values are median ± CI. *$P < 0.05$; **$P < 0.01$; ***$P < 0.001$ vs. vehicle.

Downloaded from journals.physiology.org/journal/ajplung at Midwestern Univ Lib (132.174.254.157) on December 20, 2022.

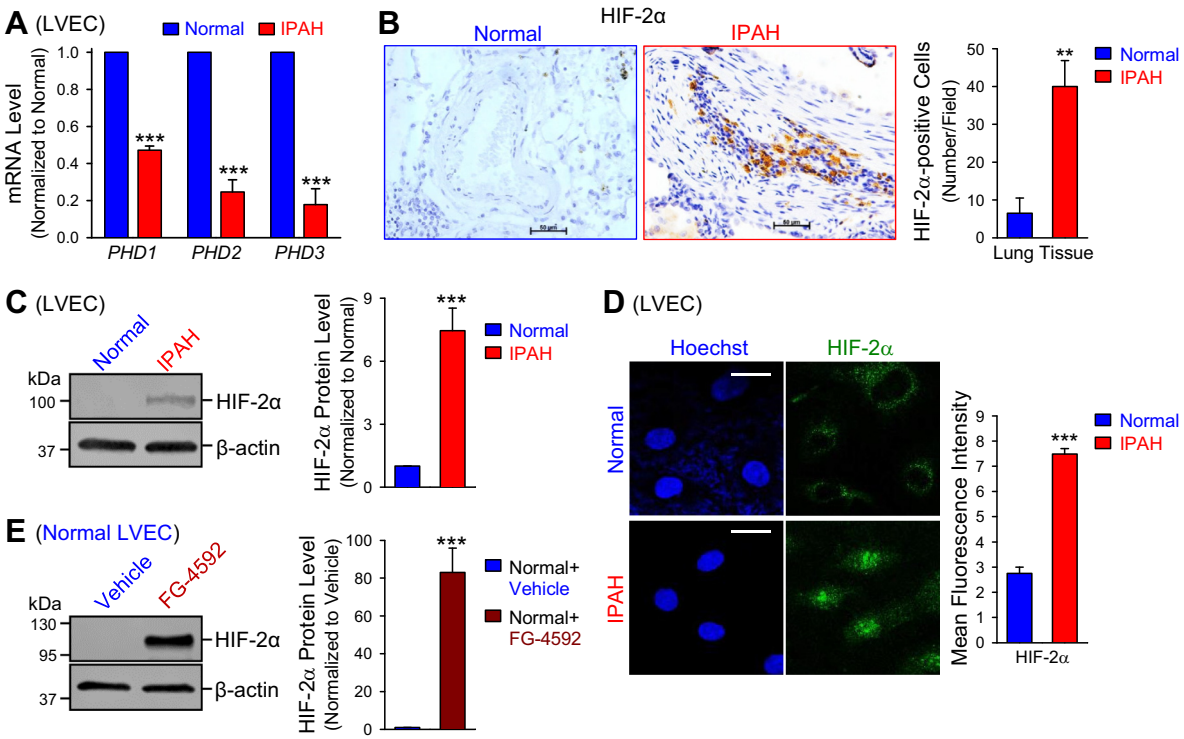

Fig. 3. Expression of prolyl hydroxylase domain protein 2 (PHD2) is decreased, and hypoxia-inducible factor 2α (HIF-2α) is increased in pulmonary arterial (PA) endothelium and LVECs from patients with IPAH. *A*: real-time RT-PCR analysis of *PHD1/2/3* (normalized to *GAPDH* expression) in LVECs from normal subjects ($n = 7$) and patients with IPAH ($n = 6$). *B*: representative images (panels at *left*) showing immunohistochemical staining for HIF-2α in distal pulmonary arteries and summarized data (panel at *right*) in normal subjects and IPAH patients. Scale bars, 50 μm. *C*: representative Western blot images showing the protein expression level of HIF-2α (*left*) and summarized data (*right*) in LVECs from normal subjects and IPAH patients ($n = 3$ per group). *D*: representative images (*left*) and summarized data (*right*) showing the mean fluorescence intensity in normal and IPAH-LVECs stained for HIF-2α (green) ($n = 3$ per group; for each experiment, we analyzed 3 fields per view; 10 regions of interest per field of view). Nuclei counterstained with Hoechst (blue). Scale bars, 20 μm. Values are means ± SE $^{**}P < 0.01$; $^{***}P < 0.001$ vs. normal. *E*: representative Western blot images showing the protein expression level of HIF2α (*left*) and summarized data (*right*) in normal human LVECs treated with a PHD2 inhibitor (FG-4592) at a concentration of 100 μM or vehicle (0.01% DMSO) for 4 h ($n = 3$ per group). All blots were reprobed for β-actin as a loading control. Values are means ± SE $^{***}P < 0.001$ vs. vehicle.

results indicate that EndMT can be induced in normal LVECs and that this transforms the cells to have molecular and phenotypic characteristics that mimic LVECs from IPAH patients.

Downregulated PHD2 and upregulated HIF-2α are correlated with EndMT in LVECs. To determine if PHD and HIF play a role in the observed EndMT seen in LVECs from patients with IPAH, we compared the mRNA expression level of PHDs in normal and IPAH-LVECs. As shown in Fig. 3*A*, the mRNA expression levels of *PHD 1/2/3* in cells from IPAH patients was significantly lower than in normal LVECs. A significantly higher level of HIF-2α in the intraluminal occlusions and the endothelium was found in lung tissue isolated from IPAH patients (Fig. 3*B*) and in LVECs from IPAH patients (Fig. 3, *C* and *D*). As shown in Fig. 3*D*, the immunocytochemistry experiments showed that HIF-2α in the nuclei of IPAH-LVECs was significantly higher than in normal LVECs.

Although all PHD isoforms have similar functions, PHD2 is the main regulator of HIF level and the essential isoform to regulate angiogenesis in adult mice (4, 71). Consistent with this, pharmacological inhibition of PHD2 (and other PHD isoforms) with 100 μM of FG-4592 (also known as Roxadustat), a potent small-molecule inhibitor of PHD2 (41), for 4 h significantly increased HIF-2α protein level in normal LVECs (Fig. 3*E*). These results indicate that PHD2/HIF-2α signaling pathway is correlated with EndMT in LVECs isolated from IPAH patients, and inhibition of PHD2 alone is sufficient to increase HIF-2α in normal LVECs.

HIF-2α, but not HIF-1α, upregulates SNAI1/2 in LVECs isolated from IPAH patients. To study what type of cells express HIF-1α and/or HIF-12α in lung tissue isolated from normal subjects and IPAH patients, we compared the protein level of HIF-1α and HIF-2α in normal LVECs and IPAH-LVECs as well as in normal PASMCs and IPAH-PASMCs. As shown in Fig. 4, we were unable to detect HIF-1α protein in LVECs from normal subjects and IPAH patients. However, HIF-1α protein level was significantly higher in PASMCs isolated from IPAH patients than in PASMCs from normal subjects (Fig. 4*A*). The protein levels of HIF-2α were significantly increased in IPAH-LVECs compared with normal LVECs, whereas HIF-2α protein level was not significantly different between normal PASMCs and IPAH-PASMCs (Fig. 4*B*). To determine if HIF-1α and/or HIF-2α regulates SNAI1/2 in LVECs isolated from IPAH patients we transfected cells with HIF-1α or HIF-2α siRNA. Real-time RT-PCR showed that HIF-1α siRNA indeed decreased mRNA level of HIF-1α but not HIF-2α, whereas HIF-2α siRNA significantly decreased mRNA level of HIF-2α but not HIF-1α (Fig. 4*C*). Furthermore, silencing HIF-2α with siRNA significantly decreased protein level of both SNAI1 and SNAI2 transcription

Downloaded from journals.physiology.org/journal/ajplung at Midwestern Univ Lib (132.174.254.157) on December 20, 2022.

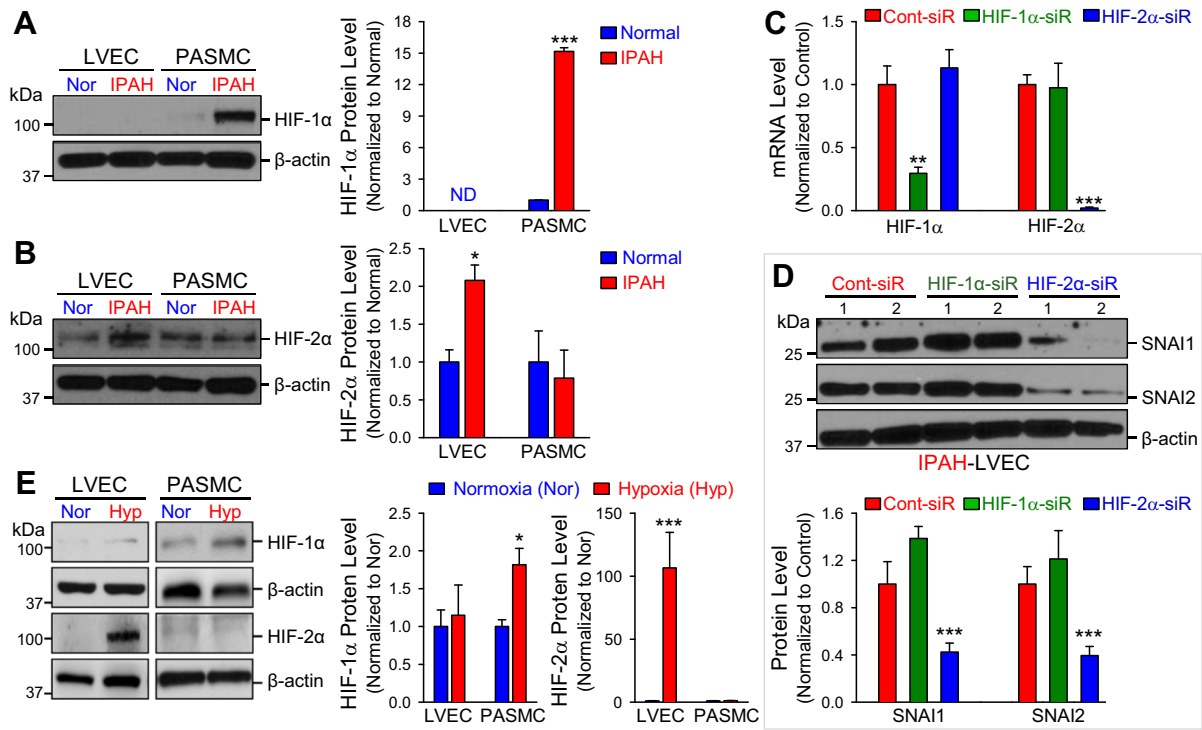

Fig. 4. HIF-2α, but not HIF-1α, regulates SNAI1/2 expression in LVECs isolated from IPAH patients. *A*: representative Western blot images showing the protein expression level of HIF-1α (*left*) and summarized data (*right*) in LVECs from seven normal subjects and six IPAH patients as well as in pulmonary arterial smooth muscle cells (PASMCs) from four normal subjects and four IPAH patients. ND, not detectable. *B*: representative Western blot images showing the protein expression level of HIF-2α (*left*) and summarized data (*right*) in normal ($n = 7$) and IPAH ($n = 6$) LVECs as well as in normal ($n = 4$) and IPAH ($n = 4$) PASMCs. Values are means ± SE; $*P < 0.05$; $***P < 0.001$ vs. normal. *C*: real-time RT-PCR analysis of HIF-1α and HIF-2α (normalized to GAPDH expression) in LVECs isolated from IPAH patients transfected with control siRNA (Cont-siR), HIF-1α siRNA (HIF-1α-siR), and HIF-2α (HIF-2α-siR) siRNA for 4–6 h ($n = 4$ per group). *D*: representative Western blot images showing the protein expression level of SNAI1 and SNAI2 (*top*) and summarized data (*bottom*) in IPAH-LVECs transfected with control, HIF-1α, and HIF-2α siRNA for 4–6 h ($n = 4$ per group). Values are means ± SE; $**P < 0.01$; $***P < 0.001$ vs. Cont-siR. *E*: representative Western blot images showing the protein expression level of HIF-1α and HIF-2α (panels at *left*) and summarized data (panels at *right*) in normal human PASMCs and human LVECs exposed to normoxia (Nor) or hypoxia (Hyp) for 48–72 h ($n = 5$ per group). All blots were reprobed for β-actin as a loading control. Values are means ± SE; $*P < 0.05$; $***P < 0.001$ vs. normoxia.

factors in IPAH-LVECs (Fig. 4*D*), whereas silencing HIF-1α in IPAH-LVECs with siRNA had no diminishing effect on SNAI1 and SNAI2 expression (Fig. 4*D*). These results indicate that HIF-2α (but not HIF-1α) is significantly increased in IPAH-LVECs under normoxic conditions in comparison to normal LVECs, whereas HIF-1α is significantly increased in IPAH-PASMCs compared with normal PASMCs. The protein expression level of HIF-1α in normal LVECs and IPAH-LVECs was too low to be detected in our experiments.

To further examine the different role of HIF-1α and HIF-2α in LVECs and PASMCs, we conducted a set of in vitro experiments to compare the protein levels of HIF-1α and HIF-2α in human (h) LVECs and PASMCs incubated under normoxic (Nor) and hypoxic (Hyp, 3% O_2) conditions. Exposure of human PASMCs to hypoxia for 48–72 h significantly increased HIF-1α protein expression without affecting the protein level of HIF-2α (Fig. 4*E*). Exposure of human LVECs to hypoxia, however, did not increase HIF-1α level, but significantly increased HIF-2α (Fig. 4*E*). These results indicate that the basal protein expression level of HIF-1α and HIF-2α in human LVECs is very low and hypoxia (for 48–72 h) selectively increases HIF-1α (but not HIF-2α) in human PASMCs and HIF-2α (but not HIF-1α) in human LVECs. Taken together, the observations from these experiments lead us to conclude that upregulated HIF-2α as a result of down-regulation of PHD2 under normoxic conditions increases the transcription factors SNAI1 and SNAI2 and, subsequently, triggers EndMT in LVECs from IPAH patients.

The next set of experiments is designed to further examine whether the endothelial HIF-2α/SNAI signaling and EndMT are also associated with the development and progression of experimental PH in animals.

EndMT is present in the lung vasculature of rats with monocrotaline-induced PH. Injection of monocrotaline (MCT) results in severe PH in rats after 2–4 wk, which has been used as an important animal model to study pathogenic mechanisms of PH and conduct drug development experiments on PH (69). Two weeks after MCT injection, the rats developed mild PH, determined by the level of RVSP and RV hypertrophy, whereas 4 wk after the injection, the animals developed severe PH (Fig. 5, *A* and *B*). Four weeks after rats had received the MCT injection, RVSP was increased by 2.6 times (from 26.7 ± 2.7 to 70.1 ± 2.7 mmHg, $P < 0.001$ vs. control) compared with the RVSP level in control rats (Fig. 5*A*). The Fulton index, or the ratio of the weight of right ventricle (RV) to the weight of left ventricle (LV) and septum (S) [RV/(LV + S)], was increased by 2.3 times in MCT-PH rats after 4 wk of MCT injection (from 0.25 ± 0.01 to 0.58 ± 0.06, $P < 0.001$ vs. control) (Fig. 5*B*). The increased RVSP and RV hypertrophy were also associated with pulmonary vascular remodeling,

Downloaded from journals.physiology.org/journal/ajplung at Midwestern Univ Lib (132.174.254.157) on December 20, 2022.

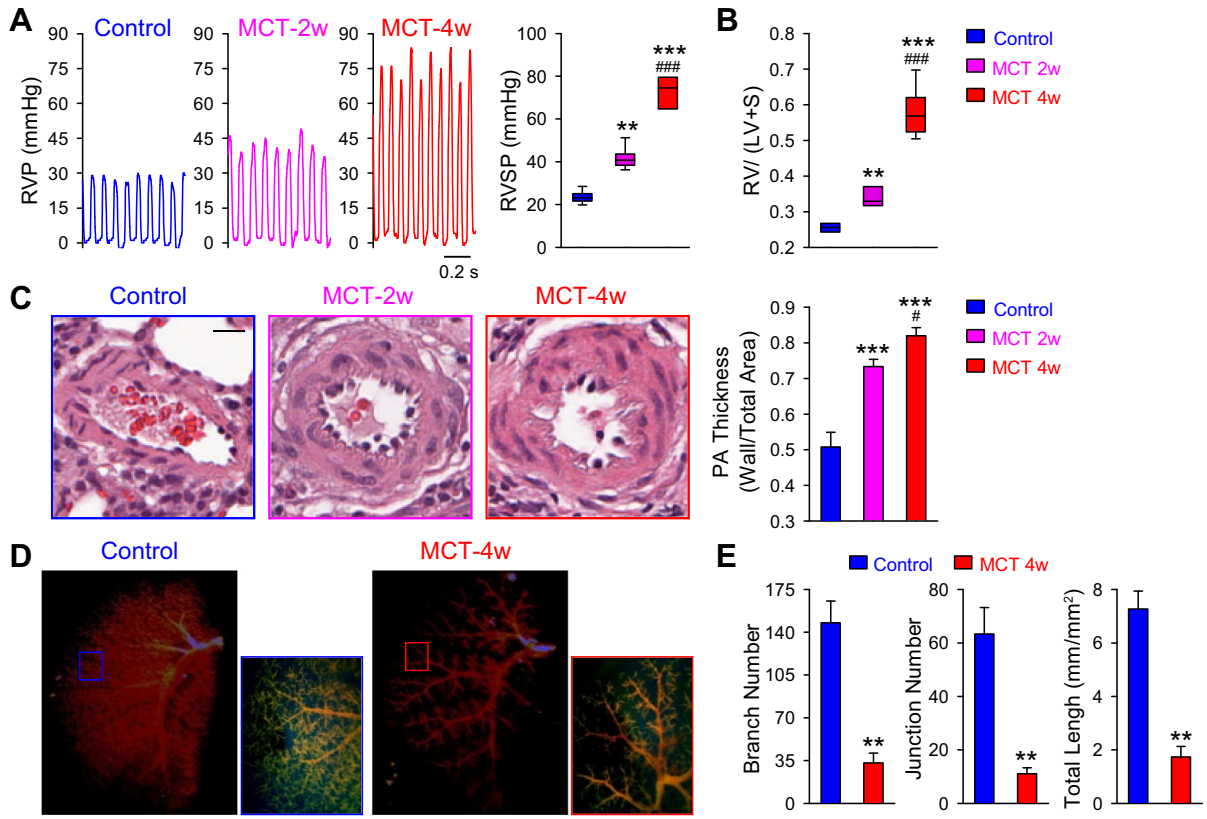

Fig. 5. Monocrotaline (MCT) treatment results in pulmonary hypertension at both 2- and 4-wk time points compared with controls. *A*: representative tracings (*left*) showing right ventricular pressure (RVP) and summarized data (*right*) showing peak right ventricular systolic pressure (RVSP) in control and treated (2 or 4 wk after MCT injection) rats. Scale bars, 0.2 s. *B*: summarized data showing RV hypertrophy defined by the Fulton index as a ratio [RV/(LV + S)] in control and MCT-treated rats (2 or 4 wk). Values are the median ± CI of individually tested rats (n = 6 per group). *C*: representative hematoxylin and eosin images of pulmonary artery (panels at *left*) and summarized data (panel at *right*) showing pulmonary artery thickness, as measured by the ratio of wall area to total vessel area in control and MCT-treated (2 or 4 wk) rats. Scale bars, 10 μm. *D*: representative angiograph images showing branches and junctions of the pulmonary arterial tree in the lungs of control and MCT-treated rats (4 wk). Insert represents the magnified area. *E*: summarized data showing the branch number, junction number, and total length of the pulmonary arterial tree measured from pulmonary angiograph images of control and MCT-treated (4 wk) animals. RVP, right ventricular pressure; RVSP, right ventricular systolic pressure; RV, right ventricle; LV, left ventricle; S, septum; PA, pulmonary artery; w, weeks. Values are the means ± SE of individually tested rat (n = 6 per group). $^{**}P < 0.01$; $^{***}P < 0.001$ vs. control; $^{\#}P < 0.05$; $^{\#\#\#}P < 0.001$ vs. MCT 2w.

determined by increased pulmonary arterial (PA) wall thickness (Fig. 5*C*) and significantly reduced lung arterial branches, junction numbers, and length in pulmonary angiography (Fig. 5, *D* and *E*). The PA thickness, normalized by the total PA cross area, was increased by 60% in MCT-PH rats after 4 wk of MCT injection (from 0.51 ± 0.04 to 0.82 ± 0.02, $P < 0.001$ vs. control) (Fig. 5*C*). The angiograph data showed that the number of branches, the number of junctions, and the total length of the vessels were decreased, respectively, by 75.7% (from 142.67 ± 11.90 to 34.6.01 ± 4.94, $P < 0.01$), 80.7% (from 60.33 ± 5.84 to 11.60 ± 1.92, $P < 0.01$), and 76.2% (from 7.27 ± 0.67 to 1.73 ± 0.39, $P < 0.01$) in MCT-PH rats after 4 wk of MCT injection (Fig. 5, *D* and *E*). These data indicate that the MCT-injected rat is a good animal model to study pathogenic mechanisms and therapeutic interventions of PH.

We investigated if EndMT was enhanced in the endothelium of remodeled small pulmonary arteries in MCT-PH rats. We observed that the intimal layer of small arteries from MCT-PH rats have significantly *1*) increased protein expression level of Snai1, *2*) decreased protein expression of Pecam1, and *3*) increased protein expression of Tagln and Acta2 (Fig. 6, *A* and *B*). Furthermore, we observed that the lung tissues (mainly contained ECs) from MCT-PH rats have significantly *1*) increased mRNA expression level of Snai1 and Snai2; *2*) decreased mRNA expression level of Pecam1, Cdh5, and catenin delta 1 (Ctnnd1, also known as p120-catenin); and *3*) increased protein expression of Acta2 and VIM (Fig. 6*C*). These data indicate that LVECs from MCT-PH rats have undergone EndMT. Similar to that observed in LVECs from patients with IPAH, the enhanced EndMT witnessed in LVECs from rats with MCT-PH was also associated with a significant increase of the cell proliferation marker Mki67 (Fig. 6*D*) and a decrease of Phd2 or Egln1 (Fig. 6*E*). These results demonstrate that LVECs in the MCT animal model of severe PH also exhibit characteristics of EndMT due potentially to downregulation of Phd2, further underscoring the importance of EndMT in the pathogenesis of severe PH.

Endothelial cell-specific deletion of the Phd2 gene, egln1, results in spontaneous pulmonary hypertension under normoxic conditions. Given that HIFs have been shown to increase expression of SNAI family members of zinc-finger transcription factors (45, 81), which are known inducers of EndMT, we sought to investigate if the PHD2/HIF-1/2α signaling pathway

Downloaded from journals.physiology.org/journal/ajplung at Midwestern Univ Lib (132.174.254.157) on December 20, 2022.

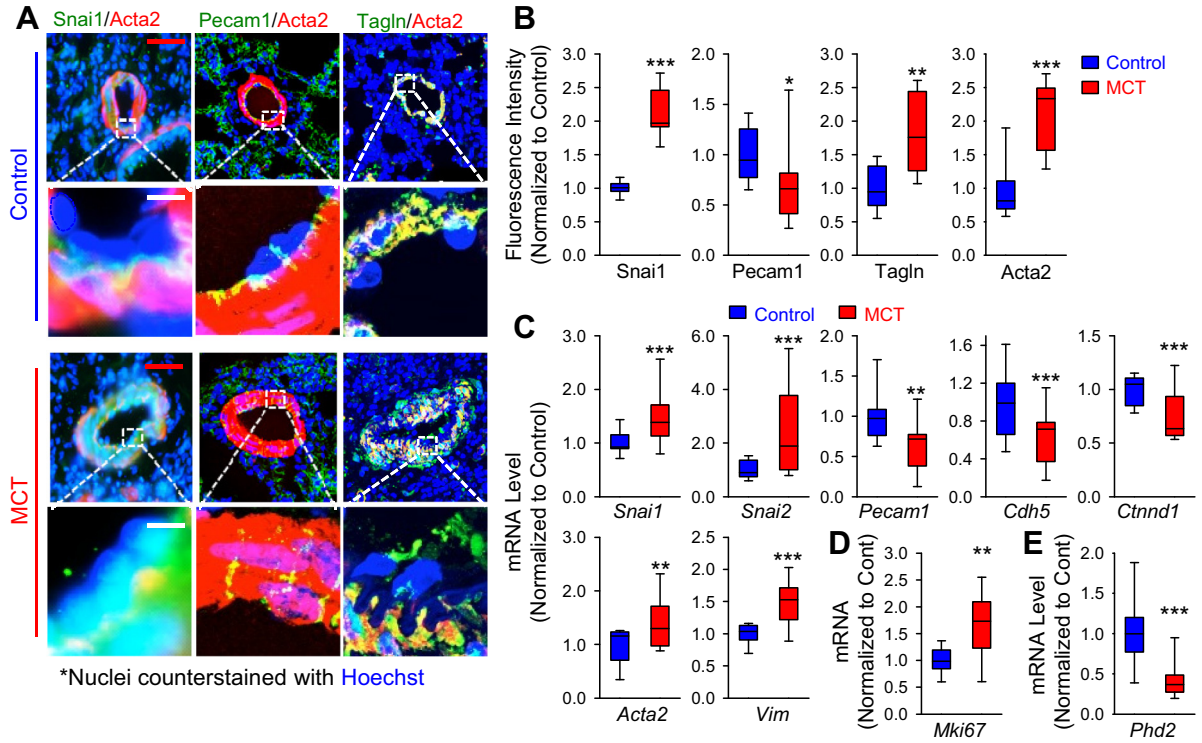

Fig. 6. EndMT observed in the lung tissue from rats with MCT-PH. *A*: representative images showing immunofluorescence of lung tissues isolated from control and MCT-treated rats stained for Snai1, Pecam1, Tagln, and Acta2. Nuclei counterstained with Hoechst. Insert represents the magnified area. Red scale bars, 500 μm; white scale bars, 50 μm. *B*: summarized data showing the mean fluorescence intensity for each antigen in control and MCT-treated rat lung tissue (n = 3 per group; for each experiment we analyzed 5 fields of view per rat). *C–E*: real-time RT-PCR analysis of *Snai1*, *Snai2*, *Pecam1*, *Cdh5*, *Ctnnd1*, *Acta2*, *Vim*, *Mki67*, and *Phd2* (normalized to *Gapdh* expression) in control and MCT-treated rat lung tissues (n = 4 per group). Values are median ± CI; *$P < 0.05$; **$P < 0.01$; ***$P < 0.001$ vs. control.

is involved in EndMT during the development and progression of severe PH. To specifically knockout the PHD2 gene (*egln1*) in ECs, we used the *Tie*-driven *egln1*$^{F/F}$ mice (i.e., *egln1*$^{EC-/-}$ mice) in this study (37, 52). The heterozygous (*egln1*$^{EC+/-}$) and homozygous (*egln1*$^{EC-/-}$) KO mice both developed PH spontaneously under normoxic conditions. The PA systolic pressure, determined by measuring RVSP, was 23.8 ± 1.6 mmHg in the WT littermates (*egln1*$^{+/+}$) (Fig. 7*A*) and 36.4 ± 1.1 and 62.7 ± 3.7 mmHg in *egln1*$^{EC+/-}$ and *egln1*$^{EC-/-}$ mice, respectively (Fig. 7*A*). The elevated RVSP in *egln1*$^{EC-/-}$ mice was also associated with significant RV hypertrophy. The Fulton index in *egln1*$^{EC+/+}$ (WT littermates), *egln1*$^{EC+/-}$, and *egln1*$^{EC-/-}$ mice was 0.22 ± 0.01, 0.29 ± 0.01 ($P < 0.01$ vs. WT), and 0.44 ± 0.02 ($P < 0.001$ vs. WT), respectively (Fig. 7*B*). In *egln1*$^{EC-/-}$ mice, we also observed severe pulmonary vascular remodeling characterized by concentric PA wall thickening and intraluminal occlusions (Fig. 7, *C* and *D*). We observed that there was approximately an 85% increase in the PA wall thickness in *egln1*$^{EC-/-}$ mice compared with WT mice (Fig. 7*D*, *left*). The lung tissues from *egln1*$^{EC-/-}$ mice exhibited 9.46 ± 2.0% of small pulmonary arteries that were completely or partially obliterated (Fig. 7*D*, *right*). Obliterative lesions were not detected (ND) in small pulmonary arteries in lung tissues from the WT (*egln1*$^{+/+}$) mice (Fig. 7*D*, *right*). In *egln1*$^{EC-/-}$ mice, the protein (Fig. 7*E*) and mRNA (Fig. 7*F*) expression of Phd2 in lung tissues was indeed significantly lower than in the WT mice. The heterozygous *egln1*-KO (*egln1*$^{EC+/-}$) mice also had significantly reduced *Phd2* or *Egln1* mRNA expression as compared with WT mice (Fig. 7*F*).

As expected, deletion of *egln1* in ECs resulted in increased expression of HIF-2α in freshly isolated mouse LVECs under normoxic conditions (Fig. 7, *G* and *H*). In our immunocytochemistry experiments, we observed that HIF-2α in the nucleus was significantly higher in lung ECs isolated from WT mice than in lung ECs isolated from *egln1*$^{EC+/-}$ mice (Fig. 7*G*). The Western blot experiments showed that increased HIF-2α protein level in lung ECs isolated from *egln1*$^{EC+/-}$ mice was associated with a significant decrease in the protein level of Phd2 (Fig. 7*H*). These data indicate that endothelial-specific KO of the PHD2 gene, *egln1*, induces severe PH and RV hypertrophy in mice, due obviously to concentric PA wall thickening and occlusive PA intimal lesions. The increased HIF-2α in lung ECs, which upregulates the transcription factors Snai1 and Snai2 that triggers EndMT, is potentially a critical mechanism involved in the development and progression of PH in *egln1*$^{EC-/-}$ mice.

Endothelial-specific deletion of the Phd2 gene, egln1, results in EndMT associated with obliterative pulmonary vascular lesions. As described earlier, downregulation of *PHD2* and the resultant increase in HIF-2α in LVECs are associated with the development and progression of pulmonary vascular remodeling in patients with IPAH. Increased expression of HIF-2α was found in LVECs freshly isolated from *egln1*$^{EC+/-}$ mice under normoxic conditions (Fig. 7*H*). Furthermore, enhanced EndMT, determined by upregulation of *SNAI* genes and mesenchymal marker genes (e.g., *Acta2*, *Tagln*, *Vim*, *Fn1*, and *S100A4*) and downregulation of endothelial markers (e.g., Pecam1, Cdh5,

Downloaded from journals.physiology.org/journal/ajplung at Midwestern Univ Lib (132.174.254.157) on December 20, 2022.

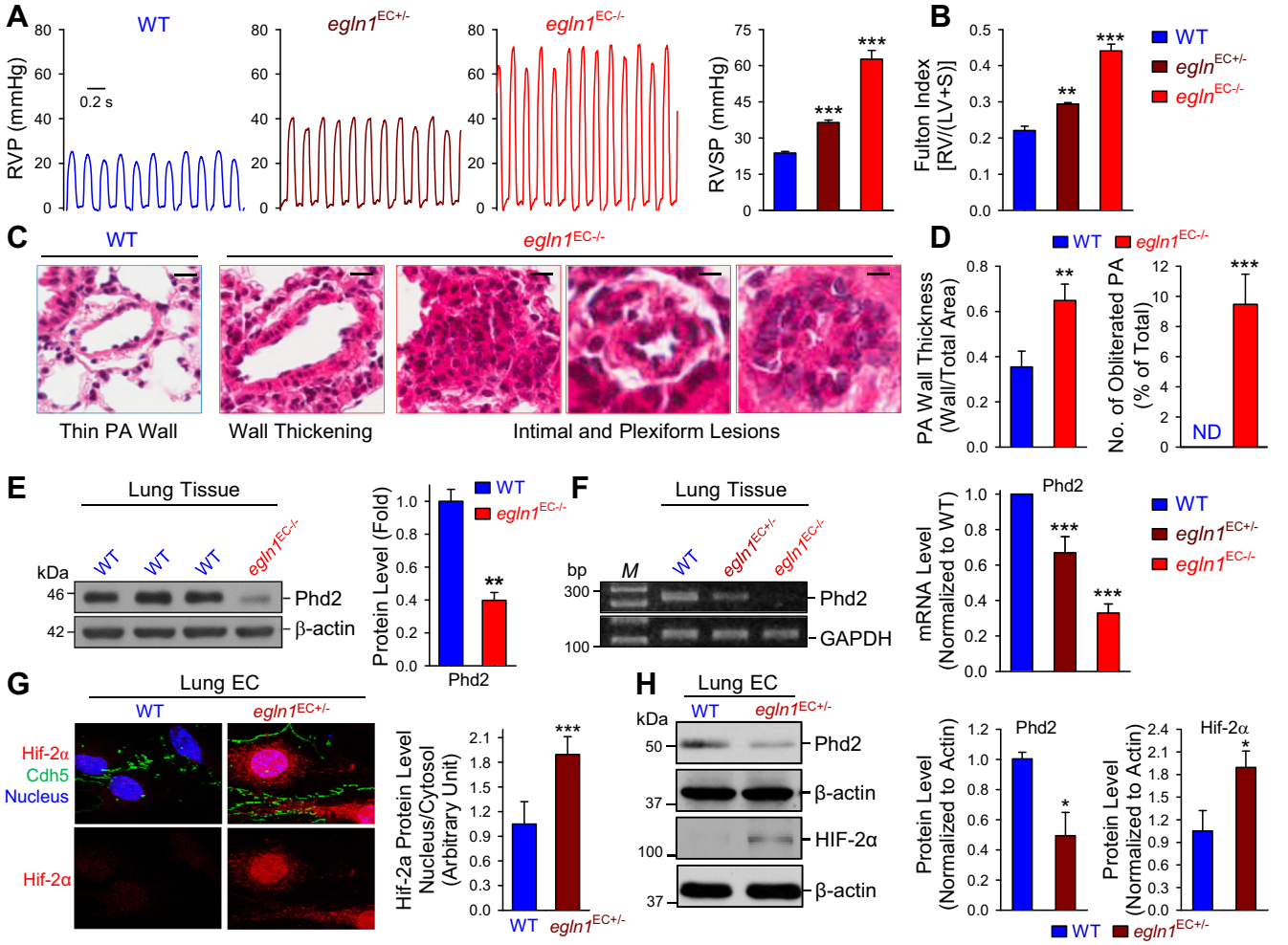

Fig. 7. Deletion of *egln1* in endothelial cells results in severe pulmonary hypertension. *A*: representative tracings (panels at *left*) showing RVP and summarized data (panel at *right*) showing peak RVSP in WT, *egln1*$^{EC+/-}$, and *egln1*$^{EC-/-}$ mice (n = 10 per group). Scale bars, 0.2 s. *B*: summarized data showing RV hypertrophy defined by the Fulton index as a ratio [RV/(LV + S)] in WT, *egln1*$^{EC+/-}$, or *egln1*$^{EC-/-}$ mice (n = 10 per group). *C*: representative hematoxylin and eosin images of small pulmonary arteries from WT mice or *egln1*$^{EC-/-}$ mice. Scale bars, 10 μm. *D*: summarized data showing PA wall thickness, as measured by the ratio of wall area to total vessel area (*left*) and the number of PA with complete obliteration or plexiform lesion (*right*) in PA with a diameter less than 100 μm from WT mice or *egln1*$^{EC-/-}$ mice (n = 10 per group). *E*: representative Western blot images (*left*) showing the protein expression level of Phd2 and summarized data (*right*) in WT and *egln1*$^{EC-/-}$murine lung tissue (n = 4 per group). *F*: representative gel images (*left*) and real-time RT-PCR analysis (*right*) of *Phd2* (normalized to *Gapdh* expression) in WT, *egln1*$^{EC+/-}$, *and egln1*$^{EC-/-}$ mouse lung tissue (n = 4 per group). *G*: representative images (*left*) and summarized data (*right*) showing immunofluorescence of lung ECs isolated from WT and *egln1*$^{EC+/-}$ mice stained for Hif-2α and Cdh5 (n = 3 per group). Nuclei counterstained with Hoechst. Scale bars, 10 μm. *H*: representative Western blot images (*left*) showing the protein expression level of Phd2 and Hif-2α and summarized data (*right*) in lung ECs isolated from WT and *egln1*$^{EC+/-}$ mouse lung tissue (n = 3 per group). All blots were reprobed for β-actin as a loading control. RVP, right ventricular pressure; RVSP, right ventricular systolic pressure; RV, right ventricle; LV, left ventricle; S, septum; PA, pulmonary artery; ND, not detectable; WT, wild-type; EC, endothelial cells. Values are means ± SE *P < 0.05; **P < 0.01; ***P < 0.001 vs. WT.

and Ctnnd1), was found to be associated with the development and progression of severe PH in patients with IPAH and animals with MCT-PH. It is unknown how increased endothelial HIF-2α results in severe PH and how endothelial HIF-2α is involved in activating EndMT to cause severe pulmonary vascular remodeling and PH in *egln1*$^{EC-/-}$ mice.

HIF-2α is known to transcriptionally upregulate *SNAI* genes, which subsequently induces EndMT (45). Indeed, markers of EndMT (i.e., Snai1 and Snai2) in the lung tissues of *egln1*$^{EC-/-}$ mice were significantly increased in comparison to the WT littermates. As shown in Fig. 8, the endothelium of small PA and the PA with occlusive intimal lesions from *egln1*$^{EC-/-}$ mice exhibited significantly *1*) increased protein expression level of Snai1 and Snai2, *2*) increased protein expression of Tagln and Acta2, and *3*) increased expression of S100A4 (Fig. 8, *A* and *B*). Furthermore, the lung tissues (mainly contained ECs) from *egln1*$^{EC-/-}$ mice exhibited significantly *1*) increased mRNA expression level of Snai1 and Snai2, *2*) decreased mRNA expression level of Pecam1 and Cdh5, *3*) increased protein expression of Acta2, and *4*) increased expression of S100A4 (Fig. 8*C*). These data indicate that deletion of the PHD2 gene, *egln1*, in lung ECs and the subsequent upregulation of HIF-2α result in EndMT to contribute to the development and progression of pulmonary vascular wall thickening and occlusive intimal lesions in severe PH.

Endothelial cell-specific deletion of hif2a prevents mice from developing pulmonary hypertension under hypoxic conditions. To determine if endothelial HIF-1α and/or HIF-2α are neces-

Downloaded from journals.physiology.org/journal/ajplung at Midwestern Univ Lib (132.174.254.157) on December 20, 2022.

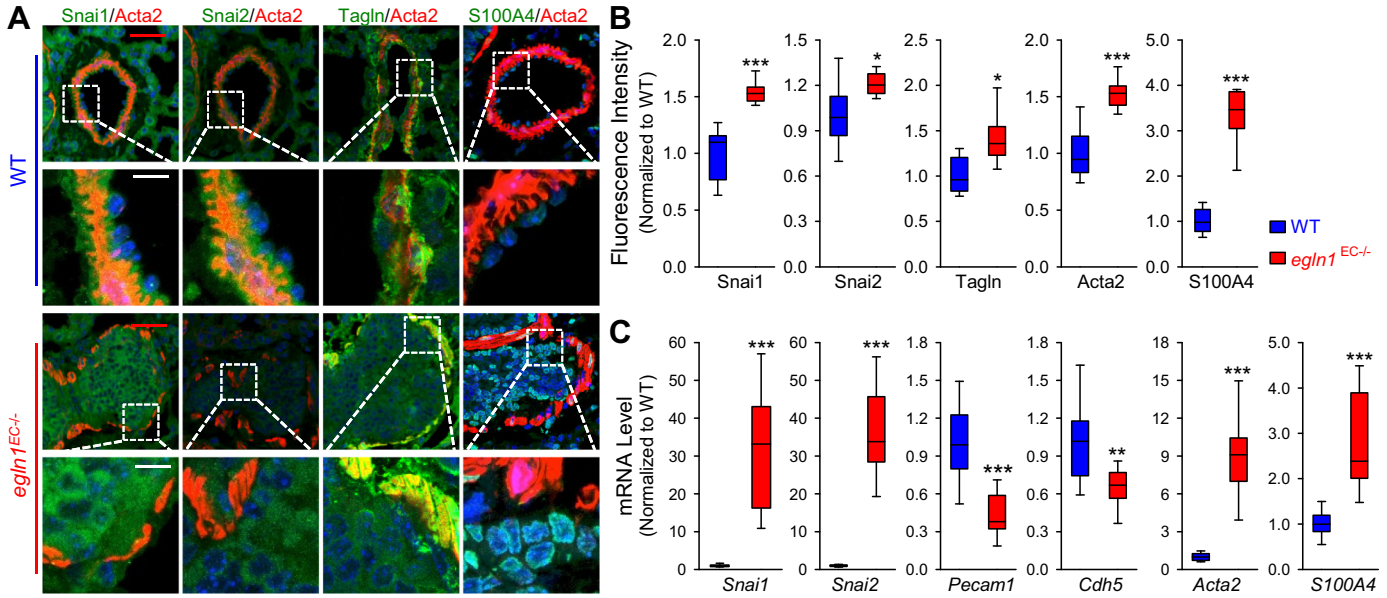

Fig. 8. EndMT observed in lung tissue of mice with endothelial-specific deletion of Phd2. *A*: representative images showing immunofluorescence of lung tissues isolated from WT (*egln1*$^{+/+}$) and *egln1*$^{EC-/-}$ mice stained for Snai1, Snai2, Tagln, Acta2, and S100A4. Nuclei counterstained with Hoechst. Insert represents the magnified area. Red scale bars, 200 μm. White scale bars, 50 μm. *B*: summarized data showing the mean fluorescence intensity for each antigen in WT and *egln1*$^{EC-/-}$ murine lung tissue ($n = 3$ per group; for each experiment, we analyzed 5 fields of view per mouse). *C*: real-time RT-PCR analysis of *Snai1*, *Snai2*, *Pecam1*, *Cdh5*, *Acta2*, and *S100A4* (normalized to *Gapdh* expression) in WT (*egln1*$^{+/+}$) or *egln1*$^{EC-/-}$ murine lung tissue ($n = 4$ per group). Values are median ± CI. *$P < 0.05$; **$P < 0.01$; ***$P < 0.001$ vs. WT.

sary for the development and progression of experimental PH, we measured and compared RVSP, Fulton index, and PA wall thickness in WT, *hif1a*$^{EC-/-}$, and *hif2a*$^{EC-/-}$ mice. As shown in Fig. 9, there was no significant difference of RVSP, Fulton index, and PA wall thickness between WT littermates (*hif2a*$^{+/+}$) and *hif2a*$^{EC-/-}$ mice under normoxic conditions (Fig. 9, *A–D*). Exposure of WT mice to hypoxia (10% O_2 for 3 wk) significantly increased RVSP (Fig. 9, *A* and *B*), enhanced RV hypertrophy determined by the Fulton index (Fig. 9*C*), and resulted in significant PA wall thickening (Fig. 9*D*).

Endothelial-specific deletion of *hif2a* (*hif2a*$^{EC-/-}$) significantly attenuated or abolished the hypoxia-induced increases in RVSP, Fulton index, and PA wall thickness in *hif2a*$^{EC-/-}$ mice (Fig. 9, *A–D*). Smooth muscle-specific deletion of *hif2a*, however, had no effect on the hypoxia-mediated PH (Fig. 9, *E–G*). Chronic exposure to normobaric hypoxia (10% O_2 for 3 wk) significantly increased RVSP (from 21.43 ± 1.30 to 39.64 ± 0.70 mmHg, $P < 0.001$) and the Fulton index (from 0.23 ± 0.01 to 0.38 ± 0.01, $P < 0.01$), respectively, in WT mice (Fig. 9, *E–G*). In *hif2a*$^{SM-/-}$ mice, hypoxic exposure also significantly increased RVSP (from 20.57 ± 0.90 to 39.46 ± 1.50 mmHg, $P < 0.001$) and the Fulton index (from 0.24 ± 0.01 to 0.40 ± 0.02, $P < 0.01$), respectively (Fig. 9, *E–G*). There was no significant difference in the hypoxia-induced increases in RVSP and Fulton index between WT and *hif2a*$^{SM-/-}$ mice (Fig. 9, *F* and *G*). These data indicate that smooth muscle-specific KO of the *HIF-2α* gene, *hif2a*, has no protective effect of hypoxia-induced PH in mice.

Furthermore, we also examined whether endothelial-specific KO of the HIF-1α gene, *hif1a*, ameliorate the development and progression of PH under hypoxic condition. Three weeks of exposure to normobaric hypoxia significantly increased RVSP (from 22.50 ± 1.30 to 38.00 ± 0.90 mmHg, $P < 0.001$) and the Fulton index (from 0.25 ± 0.02 to 0.39 ± 0.03, $P < 0.01$), respectively, in WT mice (Fig. 9, *H–J*). In *hif1a*$^{EC-/-}$ mice, hypoxic exposure also significantly increased RVSP (from 22.00 ± 0.70 to 36.50 ± 1.50 mmHg, $P < 0.001$) and the Fulton index (from 0.25 ± 0.01 to 0.36 ± 0.03, $P < 0.01$), respectively (Fig. 9, *H–J*). There was no significant difference in the hypoxia-induced increases in RVSP and Fulton index between WT and *hif1a*$^{EC-/-}$ mice (Fig. 9, *I* and *J*). These data indicate that EC-specific KO of the *HIF-1α* gene, *hif1a*, has no protective effect of hypoxia-induced PH in mice. The inability of chronic hypoxia to cause PH and RV hypertrophy in only *hif2a*$^{EC-/-}$ mice (but not in *hif2a*$^{SM-/-}$ or *hif1a*$^{EC-/-}$ mice) indicates that upregulated HIF-2α expression in pulmonary vascular ECs plays an important pathogenic role in the development and progression of PH.

Endothelial deletion of hif1a or hif2a has no effect on acute hypoxia-induced pulmonary vasoconstriction. To investigate whether endothelial HIF-2α is also involved in the regulation of pulmonary vasoconstrictive response to contractile stimuli or pulmonary vascular reactivity, we determined and compared the high K^+-mediated vasoconstriction and alveolar hypoxia-induced vasoconstriction in isolated perfused/ventilated lungs from WT and *hif2a*$^{EC-/-}$ mice. As shown in Fig. 10, intrapulmonary perfusion of solutions containing 10, 20, 30, 40, 60, 80, and 120 mM K^+, caused a dose-dependent increase in PAP (Fig. 10*A*). The amplitudes of the high K^+-induced increases in PAP at different doses and the EC_{50} of the high K^+-induced increases in PAP in isolated perfused/ventilated lungs from WT littermates were both comparable to those in isolated perfused/ventilated lungs from *hif1a*$^{EC-/-}$ and *hif2a*$^{EC-/-}$ mice (Fig. 10, *A* and *B*). As shown in Fig. 10*B*, the dose-response curves of the high K^+-induced increases in PAP obtained from isolated per-

Downloaded from journals.physiology.org/journal/ajplung at Midwestern Univ Lib (132.174.254.157) on December 20, 2022.

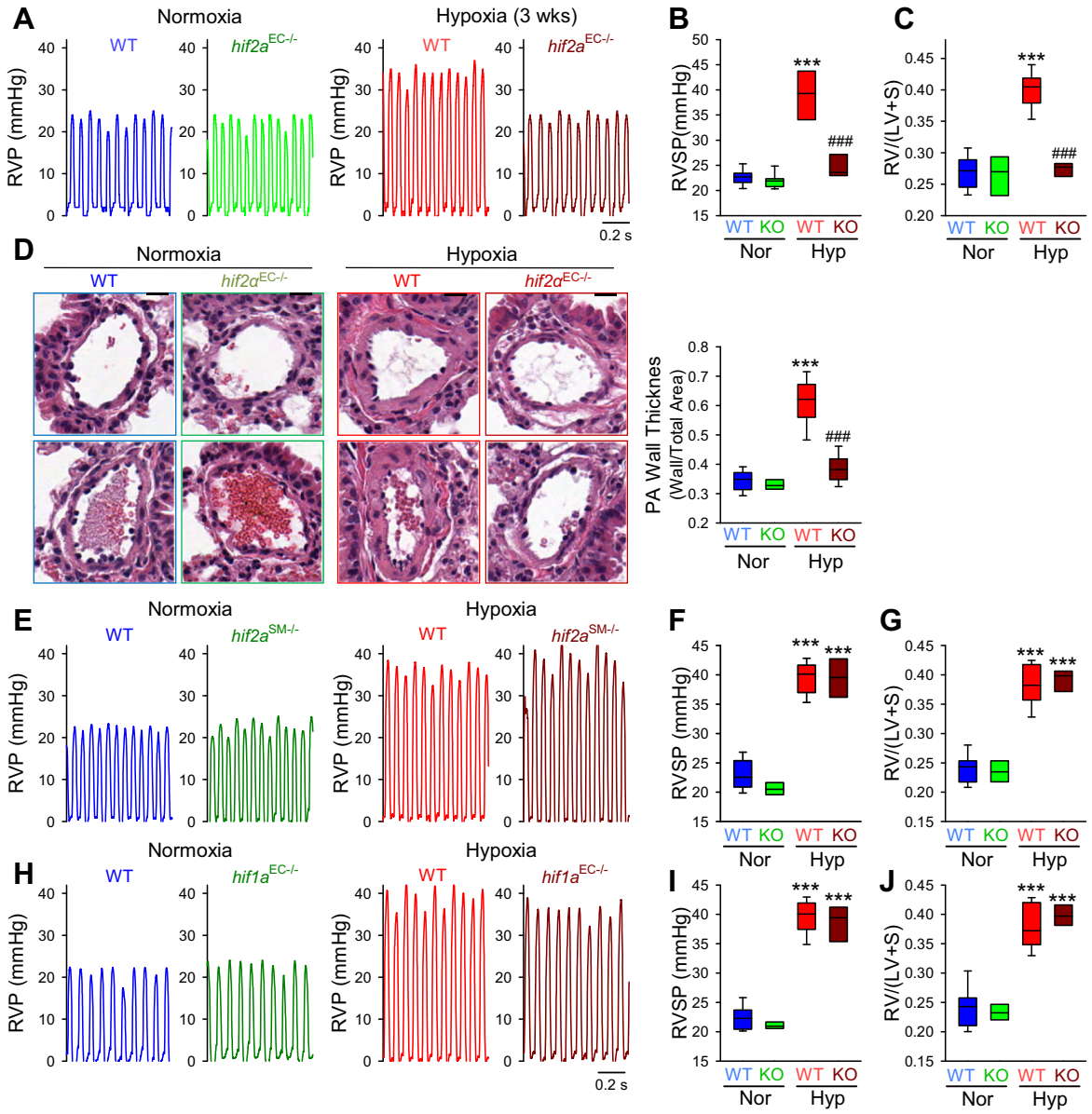

Fig. 9. Endothelial-specific deletion of *hif2α* attenuates hypoxia-induced pulmonary hypertension. Representative tracings showing RVP (*A*) and summarized data (*B*) showing peak RVSP in WT and *hif2a*$^{EC-/-}$ mice (KO) in both normoxia and hypoxia for 3 wk. Scale bar, 0.2 s. *C*: summarized data showing right ventricle hypertrophy defined by the Fulton index as a ratio [RV/(LV + S)] in WT and *hif2a*$^{EC-/-}$ mice under normoxic and hypoxic conditions. *D*: representative hematoxylin and eosin images of distal pulmonary arteries (*left*) and summarized data (*right*) showing PA wall thickness, as measured by the ratio of wall area to total vessel area, in WT and *hif2a*$^{EC-/-}$ (KO) mice in normoxic and hypoxic conditions for 3 wk. Scale bars, 10 μm. Representative tracings showing RVP (*E*) and summarized data showing peak RVSP (*F*) and RV hypertrophy (*G*) in WT and *hif2a*$^{SM-/-}$ mice (KO) under normoxia or hypoxia (for 3 wk). Representative tracings showing RVP (*H*) and summarized data showing peak RVSP (*I*) or RV hypertrophy (*J*) in WT and *hif1a*$^{EC-/-}$ mice (KO) under normoxia or hypoxia (for 3 wk). Scale bar, 0.2 s. Nor, normoxia; Hyp, hypoxia; RVP, right ventricular pressure; RVSP, right ventricular systolic pressure; RV, right ventricle; LV, left ventricle; S, septum; PA, pulmonary artery; WT, wild-type; KO, knockout. Values are the median ± CI of individually tested mice (n = 10 per group). ***$P < 0.001$ vs. WT-Nor; ###$P < 0.001$ vs. WT-Hyp.

fused/ventilated lungs of *hif1a*$^{EC-/-}$ and *hif2a*$^{EC-/-}$ mice overlap with the curves obtained from the respective WT mice.

The alveolar hypoxia (by ventilation of 3% O_2 via a mini ventilator) reversibly increased PAP in isolated perfused/ventilated lungs from WT mice; the amplitude of acute hypoxia-induced increase in PAP (4.1 ± 0.3 mmHg) was ~16% of the high K^+-induced increase in PAP at the maximal dose (24.5 ± 0.3 mmHg) (Fig. 10*C*). Endothelial-specific deletion of the HIF-1α gene, *hif1a* (*hif1a*$^{EC-/-}$), or the HIF-2α gene, *hif2a* (*hif2a*$^{EC-/-}$), had no effect on the acute hypoxia-induced increase in PAP (Fig. 10, *A*, shadowed, and *C*). Neither HIF-1α nor HIF-2α in pulmonary vascular ECs appear to be involved in the regulation of acute hypoxia-induced pulmonary vasoconstriction. Taken together, these data indicate that endothelial HIF-2α (but not HIF-1α) plays an important role in the development and progression of PH by contributing to concentric pulmonary vascular remodeling and obliterative pulmonary vascular intimal lesions rather than via increased vasoconstriction.

Downloaded from journals.physiology.org/journal/ajplung at Midwestern Univ Lib (132.174.254.157) on December 20, 2022.

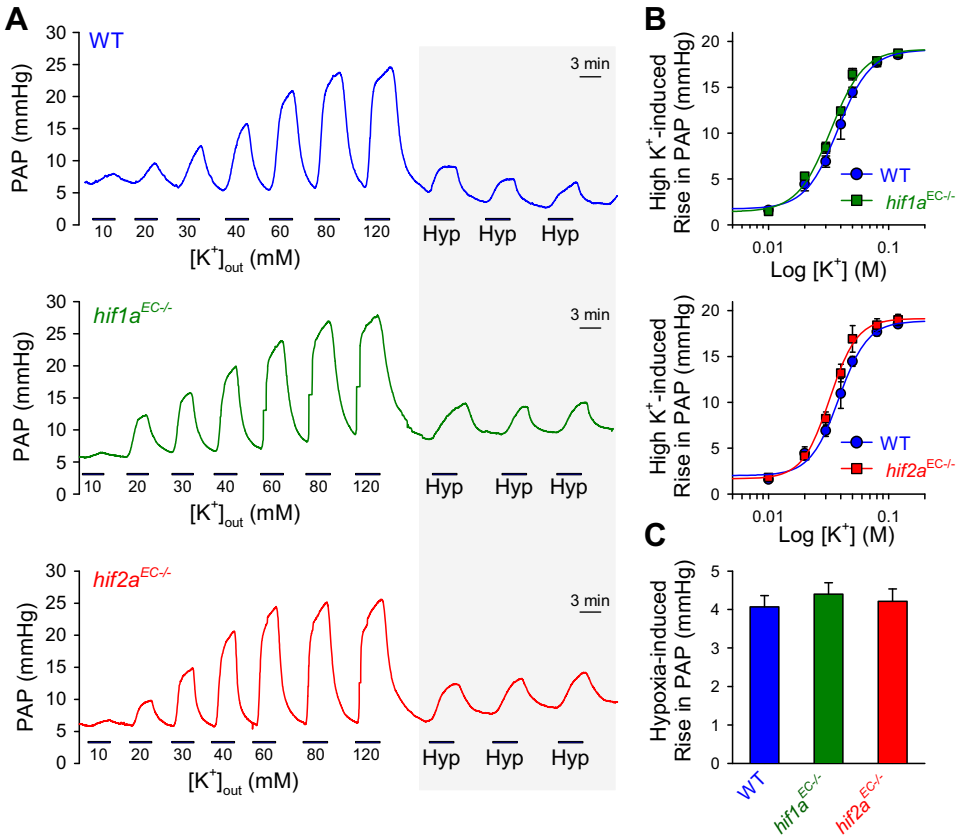

Fig. 10. Deletion of *hif1a* or *hif2a* in endothelial cells has no effect on acute hypoxia-induced pulmonary vasoconstriction. *A*: representative tracings showing pulmonary artery pressure (PAP) before, during (solid bar), and after superfusion of modified Kreb's solutions with different K^+ concentrations (10, 20, 30, 40, 60, 80, or 120 mM) and airway ventilation of hypoxia (Hyp) (solid bar; 1% O_2; shadowed) in isolated perfused/ventilated lungs from wild-type (WT) (*top*), $hif1a^{EC-/-}$ (*middle*), or $hif2a^{EC-/-}$ (*bottom*) mice. Scale bars, 3 min. *B*: summarized data showing dose-response curves of high K^+-induced increases in mean PAP in isolated perfused/ventilated lungs from eight WT, four $hif1a^{EC-/-}$, or four $hi2a^{EC-/-}$ mice. *C*: summarized data showing amplitudes of hypoxia-induced increases in mean PAP in isolated perfused/ventilated lungs from WT, $hif1a^{EC-/-}$, or $hif2a^{EC-/-}$ mice. Values are means ± SE. No significant differences were seen between WT and $hif1a^{EC-/-}$ or $hif2a^{EC-/-}$ mice.

DISCUSSION

In this study, our results demonstrate the following: *1*) LVECs isolated from patients with IPAH and animals with experimental PH exhibited high level of EndMT (characterized by increased SNAI1 and SNAI2, downregulated PECAM1 and CHD5, upregulated ACTA2 and TAGLN, and upregulated S100A4 and FN1, and were highly proliferative (characterized by increased EdU incorporation and Mki67 expression) in comparison to LVECs isolated from normal controls; *2*) protein expression level of HIF-2α in LVECs from IPAH patients was significantly greater than in LVECs from normal controls, and the upregulated HIF-2α in IPAH-LVECs was associated with a decreased protein level of PHD2, a hydroxylase that promotes HIF degradation; *3*) downregulation of HIF-2α in LVECs from IPAH patients with siRNA leads to decrease in protein level of SNAI1 and SNAI2, two transcription factors involved in initiating EndMT; *4*) mice ($egln1^{EC-/-}$) with EC-specific KO of the PHD2 gene, *egln1*, spontaneously develop severe PH characterized by excessive pulmonary vascular remodeling and occlusive lesions as a result of increased protein level of HIF-2α and enhanced translocation of HIF-2 to the nucleus in LVECs; *5*) LVECs from $egln1^{EC-/-}$ mice exhibited high level of EndMT in comparison to LVECs from the WT littermates ($egln1^{EC+/+}$); and *6*) endothelial-specific KO of the HIF-2α gene, *hif2a*, ameliorates the development and progression of experimental PH in mice ($hif2a^{EC-/-}$) compared with the WT control mice ($hif2a^{EC+/+}$). These observations provide compelling evidence that EndMT, due likely to the Hif-2-mediated upregulation of Snai1/Snai2, plays an important pathogenic role in the development and progression of concentric pulmonary vascular wall thickening and occlusive pulmonary vascular intimal lesions. Inhibition of the HIF-mediated EndMT in LVECs would thus be a novel approach to develop novel therapies for severe pulmonary hypertension.

EndMT is a process by which ECs reprogram to acquire a mesenchymal phenotype in association with upregulation of SMC-specific and/or fibroblast-specific genes and downregulation of EC-specific genes. SNAI1 and SNAI2 are two structurally related transcription factors that initiate EndMT (39). EndMT enables slowly growing ECs to reprogram to a highly proliferative mesenchymal cell phenotype such as myofibroblasts or fibroblasts (2, 47). EndMT has been implicated during the development and progression of pulmonary vascular remodeling in patients with IPAH and animals with experimental PH (19, 28, 30, 60). In the present study, we demonstrated that EndMT was enhanced in LVECs from IPAH patients and that normal LVECs from healthy donors can be induced to undergo EndMT by in vitro treatment with TGF-β1. The increased expression of TGF-β isoforms has been found in pulmonary arteries from patients with IPAH (7). In addition to the enhanced EndMT in LVECs isolated from IPAH patients, we also demonstrated that EndMT was enhanced in rats with MCT-induced PH. The MCT-PH model was chosen for this study because it is associated with severe pulmonary vascular remodeling, including progressive obstruction of small arteries and precapillary arterioles (50, 69). Interestingly, that TGF-β has been shown to be particularly upregulated in the MCT model (3, 12, 47). We observed that ECs in lung tissue from MCT-PH rats undergoes EndMT, similar to that seen in IPAH-LVECs. Although inflammation plays a critical role in the

Downloaded from journals.physiology.org/journal/ajplung at Midwestern Univ Lib (132.174.254.157) on December 20, 2022.

development of pulmonary vascular remodeling through different mechanisms, a recent report demonstrates that inflammation induces EndMT via upregulation of SNAI1 and SNAI2 downstream of TGF-β1, TNF-α, and IL-1β (62). We also showed that TGF-β1 induced EndMT in LVECs and therefore may contribute to the development and progression of pulmonary vascular remodeling in PAH.

Moreover, LVECs from IPAH patients and MCT-PH rats had higher proliferation rate compared with controls, which indicate that EndMT may be a source of highly proliferative ECs. There are also other mechanisms involved in the controlling of LVEC proliferation and differentiation, for example, BMPR2 signaling. Recent findings revealed the complex cross talk between BMPR2 and TGF-β signaling pathways. Hypoxia- and MCT-induced PH animal models display decreased BMPR2 expression and increased TGF-β expression (3, 12, 47). TGF-β1-induced EndMT was associated with reduced BMPR2 expression in vitro and in vivo and partially ameliorated by stimulating BMPR2 signaling (30, 61). These data suggest that EndMT may enhance vascular remodeling induced by the impaired BMPR2 pathway via conversion of slowly growing fully differentiated LVECs into highly proliferative mesenchymal cells.

HIF-1 and HIF-2 includes a heterodimer of an inducible subunit called HIF-α and a constitutively expressed subunit HIF-β. PHD family members hydroxylate HIF-α so that it can be recognized by the ubiquitin E3 ligase and directed to the proteasome for degradation (34, 35). HIF-α protein levels are stabilized in responsive to hypoxia, and also under normoxic conditions in response to stimuli such as growth factors, inflammatory cytokines, infectious microorganisms, and NO (64). The mechanism by which HIF-α protein levels are stabilized (or increased) involves decreased expression or decreased catalytic activity of PHD. PHD2/HIF signaling mediates adaptive molecular responses to low O_2 availability and plays an important role in the development and progression of PH (65). We propose that both HIF-1α and HIF-2α are important for the development of pulmonary hypertension, but their pathogenic roles appeared to be different in different cell types and processes. Upregulated HIF-1α in PASMCs from IPAH patients may play an important role in the development and progression of pulmonary arterial medial hypertrophy and sustained pulmonary vasoconstriction (6, 16, 31, 70, 79). Our results suggest that upregulated HIF-2α in lung ECs plays a predominant role in promoting EndMT and, potentially, occlusive intimal/neointimal lesions and severe pulmonary vascular wall thickening in IPAH. Interestingly, the findings from this study are consistent with the previous reports that HIF activation is independent of pO_2 in patients with PAH (6, 76).

Accumulating evidence demonstrates that deficiency of PHD2 leads to vascular remodeling (22, 36, 78). Indeed, we observed decreased PHD2 expression in LVECs from rats with MCT-induced PH, which is similar to that seen in LVECs isolated from IPAH patients. Previous studies revealed that TGF-β1 markedly and specifically decreases both mRNA and protein levels of PHD2 through the Smad-signaling pathway (51). Moreover, EC-specific deletion of the PHD2 gene increased the expression of TGF-β1, which indicates the positive feedback loop to maintain TGF-β1 signaling pathway (77). In this study we observed that HIF-2α protein level was elevated in IPAH-LVECs, whereas HIF-1α was upregulated in IPAH-PASMCs under normoxic conditions. Our findings are consistent with recent studies by Chae et al. (15) that demonstrated the upregulation of both HIF-α isoforms in response to TGF-β1 in nonhypoxic conditions. However, TGF-β1 induces promoter activity of vascular endothelial growth factor (VEGF) through HIF-2α, but not HIF-1α, which indicate the differential roles of HIF-α subunits in the TGF-β1 signaling pathway and the development and progression of pulmonary vascular remodeling. Recently VEGF has been established as a contributor to pulmonary vascular remodeling in LVECs (1, 44), thus further highlighting the importance of HIF-2α in the development of EndMT and obliterative pulmonary vascular lesions in PAH. Hypoxia decreases PHD2 activity, which in turn leads to stabilization of HIF-α. Endothelial-specific deletion of the PHD2 gene, *egln1*, (using *Tie2*-Cre mice) results in significant increases in HIF-2α and Snai1/Snai2 in LVECs. Additionally, $egln1^{EC-/-}$ mice exhibited severe PH under normoxic conditions associated with *1*) significant concentric PA thickening and intraluminal obliteration and *2*) a significant level of EndMT in lung vascular endothelium.

Here, in investigating the role of the PHD/HIF pathway in the formation of intraluminal occlusions, we found that deletion of the PHD2 gene, *egln1*, in ECs increased the HIF-2α by decreasing its degradation, which then activated EndMT by upregulating Snai1 and Snai2, and resulted in severe pulmonary vascular remodeling including intraluminal obliterations in $egln1^{EC-/-}$ mice. Vice versa, siRNA targeted knockdown of HIF-2α, but not HIF-1α, decreases SNAI1/2 protein expression in IPAH-LVECs. Furthermore, our results demonstrated that EC deletion of the HIF-2α gene, *hif2a*, but not EC deletion of the HIF-1α gene, *hif1a*, or SM-specific deletion of the HIF-2α gene, *hif2α*, was able to prevent mice from developing chronic hypoxia-induced PH, RV hypertrophy, and pulmonary vascular remodeling (determined by increased PA wall thickness), further emphasizing the unique role of HIF-2α in the endothelium. These results are supported by previous findings demonstrating that haploinsufficiency for *hif2a*, or endothelial-specific deletion of *hif2a*, protects mice against vascular remodeling and PH (10, 20, 29, 57). The obtained data were confirmed by in vitro experiments. We observed a hypoxia-induced increase in expression of both HIF isoforms, but in different cells, i.e., HIF-2α was exclusively elevated in LVECs, whereas HIF-1α was upregulated in PASMCs only. Given that hypoxia induces EndMT (46, 80, 81), we conclude that endothelial HIF-2α but not HIF-1α can also contribute to EndMT in hypoxia-induced PH by promoting SNAI1/2. Our results further suggest a mechanism whereby augmented PHD2/HIF-2α/SNAI signaling in LVECs contributes to the development of pulmonary vascular remodeling characterized by obliterative pulmonary vascular lesions via enhanced EndMT in LVECs.

Stabilized HIF-α leads to dimerization with HIF-β and accumulation in the nucleus where the heterodimeric complex interacts with coactivators (e.g., p300/CBP), binds to the HIF-binding site or the HIF-responsive element (5′-RCGTG-3′) in the promoter regions of various genes, and promotes transcription to enhance cell proliferation (23). The EndMT-related transcription factor SNAI1 is a direct target of HIF-α, suggesting that stabilization of HIF-α may be an upstream activator of EndMT (45, 81).

Downloaded from journals.physiology.org/journal/ajplung at Midwestern Univ Lib (132.174.254.157) on December 20, 2022.

HIF-1α and HIF-2α are structurally similar in their dimerization domains but differ in their transactivation domain. Indeed, others have shown that they have unique target genes (18, 32, 53). In human melanoma cells, high levels of HIF-2α are associated with increased metastatic capacity and poor prognosis (45). Overexpression of HIF-2α in melanoma cells significantly upregulates expression of SNAI1. In contrast, overexpression of HIF-1α has no effect on mRNA expression level of SNAI1 (45). These data imply that in some cell types, HIF-2α, but not HIF-1α, is a crucial transcription factor responsible for induction of EndMT. Furthermore, HIF-1α is expressed ubiquitously, but HIF-2α is predominantly expressed in the lung endothelium (75). Taken together with our observations in this study, we suggest that endothelial HIF-2α plays a unique pathogenic role in the development and progression of concentric pulmonary vascular wall thickening and obliterative pulmonary vascular lesions in PAH and severe PH in general.

IPAH is a fatal and progressive pulmonary vascular disease without a cure. A better understanding of the pathogenic mechanisms contributing to concentric PA wall thickening and intraluminal occlusions may provide an opportunity for developing novel drug targets and therapeutic strategies. Our studies strongly support the premise that the activation of an endothelial HIF-2α/SNAI signaling pathway is a pivotal pathogenic sequence of events that leads to severe pulmonary vascular remodeling. Combined activation of PHD2, inhibition of HIF-2α, and attenuation of EndMT in LVECs may yield a unique therapeutic approach for the treatment of IPAH and other forms of pulmonary hypertension.

ACKNOWLEDGMENTS

We are grateful for the mice provided by Drs. Guofei Zhou and Haixia Gong from the University of Illinois at Chicago and for the data/tissue samples provided by PHBI under the Pulmonary Hypertension Breakthrough Initiative (PHBI).

GRANTS

This work was supported in part by National Heart, Lung, and Blood Institute Grants HL-125208, HL-135807, HL-126609, and HL-115578. Funding for PHBI is provided under National Heart, Lung, and Blood Institute Grant R24 HL-123767 and by the Cardiovascular Medical Research and Education Fund.

DISCLOSURES

No conflicts of interest, financial or otherwise, are declared by the authors.

AUTHOR CONTRIBUTIONS

H.T., A. Babicheva, and J.X.-J.Y. conceived and designed research; H.T., A. Babicheva, K.M.M., Y.G., R.J.A., S.S., Ziyi Wang, A.G., T.Z., X.S., S.D., Zilu Wang, Q.Y.Z., A.G.C., A.A.D., F.R., Z.K., J.W., S.M.B., J.G.G., and A.M. performed experiments; H.T., A. Babicheva, K.M.M., Y.G., R.J.A., S.S., Ziyi Wang, A.G., T.Z., X.S., S.D., Zilu Wang, A. Balistrieri, Q.Y.Z., A.G.C., A.A.D., F.R., Z.K., J.W., S.M.B., J.G.G., A.M., and J.X.-J.Y. analyzed data; H.T., A. Babicheva, A. Balistrieri, and J.X.-J.Y. interpreted results of experiments; H.T., A. Babicheva, K.M.M., S.S., Ziyi Wang, A. Balistrieri, Q.Y.Z., and J.X.-J.Y. prepared figures; H.T., A. Babicheva, and J.X.-J.Y. drafted manuscript; H.T., A. Babicheva, K.M.M., A. Balistrieri, and J.X.-J.Y. edited and revised manuscript; H.T., A. Babicheva, K.M.M., Y.G., R.J.A., S.S., A.G., T.Z., X.S., S.D., Zilu Wang, A.G.C., A.A.D., F.R., Z.K., J.W., S.M.B., J.G.G., A.M., and J.X.-J.Y. approved final version of manuscript.

REFERENCES

1. **Al-Husseini A, Kraskauskas D, Mezzaroma E, Nordio A, Farkas D, Drake JI, Abbate A, Felty Q, Voelkel NF.** Vascular endothelial growth factor receptor 3 signaling contributes to angioobliterative pulmonary hypertension. *Pulm Circ* 5: 101–116, 2015. doi:10.1086/679704.
2. **Arciniegas E, Frid MG, Douglas IS, Stenmark KR.** Perspectives on endothelial-to-mesenchymal transition: potential contribution to vascular remodeling in chronic pulmonary hypertension. *Am J Physiol Lung Cell Mol Physiol* 293: L1–L8, 2007. doi:10.1152/ajplung.00378.2006.
3. **Arcot SS, Lipke DW, Gillespie MN, Olson JW.** Alterations of growth factor transcripts in rat lungs during development of monocrotaline-induced pulmonary hypertension. *Biochem Pharmacol* 46: 1086–1091, 1993. doi:10.1016/0006-2952(93)90675-M.
4. **Berra E, Benizri E, Ginouvès A, Volmat V, Roux D, Pouysségur J.** HIF prolyl-hydroxylase 2 is the key oxygen sensor setting low steady-state levels of HIF-1α in normoxia. *EMBO J* 22: 4082–4090, 2003. doi:10.1093/emboj/cdg392.
5. **Bishop T, Ratcliffe PJ.** HIF hydroxylase pathways in cardiovascular physiology and medicine. *Circ Res* 117: 65–79, 2015. doi:10.1161/CIRCRESAHA.117.305109.
6. **Bonnet S, Michelakis ED, Porter CJ, Andrade-Navarro MA, Thébaud B, Bonnet S, Haromy A, Harry G, Moudgil R, McMurtry MS, Weir EK, Archer SL.** An abnormal mitochondrial-hypoxia inducible factor-1α-Kv channel pathway disrupts oxygen sensing and triggers pulmonary arterial hypertension in fawn hooded rats: similarities to human pulmonary arterial hypertension. *Circulation* 113: 2630–2641, 2006. doi:10.1161/CIRCULATIONAHA.105.609008.
7. **Botney MD, Bahadori L, Gold LI.** Vascular remodeling in primary pulmonary hypertension. Potential role for transforming growth factor-β. *Am J Pathol* 144: 286–295, 1994.
8. **Boutin AT, Weidemann A, Fu Z, Mesropian L, Gradin K, Jamora C, Wiesener M, Eckardt KU, Koch CJ, Ellies LG, Haddad G, Haase VH, Simon MC, Poellinger L, Powell FL, Johnson RS.** Epidermal sensing of oxygen is essential for systemic hypoxic response. *Cell* 133: 223–234, 2008. doi:10.1016/j.cell.2008.02.038.
9. **Branco-Price C, Zhang N, Schnelle M, Evans C, Katschinski DM, Liao D, Ellies L, Johnson RS.** Endothelial cell HIF-1α and HIF-2α differentially regulate metastatic success. *Cancer Cell* 21: 52–65, 2012. doi:10.1016/j.ccr.2011.11.017.
10. **Brusselmans K, Compernolle V, Tjwa M, Wiesener MS, Maxwell PH, Collen D, Carmeliet P.** Heterozygous deficiency of hypoxia-inducible factor-2α protects mice against pulmonary hypertension and right ventricular dysfunction during prolonged hypoxia. *J Clin Invest* 111: 1519–1527, 2003. doi:10.1172/JCI15496.
11. **Burch TC, Watson MT, Nyalwidhe JO.** Variable metastatic potentials correlate with differential plectin and vimentin expression in syngeneic androgen independent prostate cancer cells. *PLoS One* 8: e65005, 2013. doi:10.1371/journal.pone.0065005.
12. **Burke DL, Frid MG, Kunrath CL, Karoor V, Anwar A, Wagner BD, Strassheim D, Stenmark KR.** Sustained hypoxia promotes the development of a pulmonary artery-specific chronic inflammatory microenvironment. *Am J Physiol Lung Cell Mol Physiol* 297: L238–L250, 2009. doi:10.1152/ajplung.90591.2008.
13. **Carrera S, Senra J, Acosta MI, Althubiti M, Hammond EM, de Verdier PJ, Macip S.** The role of the HIF-1α transcription factor in increased cell division at physiological oxygen tensions. *PLoS One* 9: e97938, 2014. doi:10.1371/journal.pone.0097938.
14. **Castillo-Lluva S, Hontecillas-Prieto L, Blanco-Gómez A, Del Mar Sáez-Freire M, García-Cenador B, García-Criado J, Pérez-Andrés M, Orfao A, Cañamero M, Mao JH, Gridley T, Castellanos-Martín A, Pérez-Losada J.** A new role of SNAI2 in postlactational involution of the mammary gland links it to luminal breast cancer development. *Oncogene* 34: 4777–4790, 2015. doi:10.1038/onc.2015.224.
15. **Chae KS, Kang MJ, Lee JH, Ryu BK, Lee MG, Her NG, Ha TK, Han J, Kim YK, Chi SG.** Opposite functions of HIF-α isoforms in VEGF induction by TGF-β1 under non-hypoxic conditions. *Oncogene* 30: 1213–1228, 2011. doi:10.1038/onc.2010.498.

Downloaded from journals.physiology.org/journal/ajplung at Midwestern Univ Lib (132.174.254.157) on December 20, 2022.

16. **Chen T, Zhou Q, Tang H, Bozkanat M, Yuan JX, Raj JU, Zhou G.** miR-17/20 controls prolyl hydroxylase 2 (PHD2)/hypoxia-inducible factor 1 (HIF1) to regulate pulmonary artery smooth muscle cell proliferation. *J Am Heart Assoc* 5: e004510, 2016. doi:10.1161/JAHA.116.004510.
17. **Cho YE, Basu A, Dai A, Heldak M, Makino A.** Coronary endothelial dysfunction and mitochondrial reactive oxygen species in type 2 diabetic mice. *Am J Physiol Cell Physiol* 305: C1033–C1040, 2013. doi:10.1152/ajpcell.00234.2013.
18. **Choudhry H, Schödel J, Oikonomopoulos S, Camps C, Grampp S, Harris AL, Ratcliffe PJ, Ragoussis J, Mole DR.** Extensive regulation of the non-coding transcriptome by hypoxia: role of HIF in releasing paused RNApol2. *EMBO Rep* 15: 70–76, 2014. doi:10.1002/embr.201337642.
19. **Coll-Bonfill N, Musri MM, Ivo V, Barberà JA, Tura-Ceide O.** Transdifferentiation of endothelial cells to smooth muscle cells play an important role in vascular remodelling. *Am J Stem Cells* 4: 13–21, 2015.
20. **Cowburn AS, Crosby A, Macias D, Branco C, Colaço RD, Southwood M, Toshner M, Crotty Alexander LE, Morrell NW, Chilvers ER, Johnson RS.** HIF2α-arginase axis is essential for the development of pulmonary hypertension. *Proc Natl Acad Sci USA* 113: 8801–8806, 2016. doi:10.1073/pnas.1602978113.
21. **Cowburn AS, Takeda N, Boutin AT, Kim JW, Sterling JC, Nakasaki M, Southwood M, Goldrath AW, Jamora C, Nizet V, Chilvers ER, Johnson RS.** HIF isoforms in the skin differentially regulate systemic arterial pressure. *Proc Natl Acad Sci USA* 110: 17570–17575, 2013. doi:10.1073/pnas.1306942110.
22. **Dai Z, Li M, Wharton J, Zhu MM, Zhao YY.** Prolyl-4 hydroxylase 2 (PHD2) deficiency in endothelial cells and hematopoietic cells induces obliterative vascular remodeling and severe pulmonary arterial hypertension in mice and humans through hypoxia-inducible factor-2α. *Circulation* 133: 2447–2458, 2016. doi:10.1161/CIRCULATIONAHA.116.021494.
23. **Ema M, Hirota K, Mimura J, Abe H, Yodoi J, Sogawa K, Poellinger L, Fujii-Kuriyama Y.** Molecular mechanisms of transcription activation by HLF and HIF1α in response to hypoxia: their stabilization and redox signal-induced interaction with CBP/p300. *EMBO J* 18: 1905–1914, 1999. doi:10.1093/emboj/18.7.1905.
24. **Farber HW, Miller DP, Poms AD, Badesch DB, Frost AE, Muros-Le Rouzic E, Romero AJ, Benton WW, Elliott CG, McGoon MD, Benza RL.** Five-year outcomes of patients enrolled in the REVEAL Registry. *Chest* 148: 1043–1054, 2015. doi:10.1378/chest.15-0300.
25. **Feng J, Zhang J, Jackson AO, Zhu X, Chen H, Chen W, Gui Q, Yin K.** Apolipoprotein A1 inhibits the TGF-β1-induced endothelial-to-mesenchymal transition of human coronary artery endothelial cells. *Cardiology* 137: 179–187, 2017. doi:10.1159/000464321.
26. **Frid MG, Kale VA, Stenmark KR.** Mature vascular endothelium can give rise to smooth muscle cells via endothelial-mesenchymal transdifferentiation: in vitro analysis. *Circ Res* 90: 1189–1196, 2002. doi:10.1161/01.RES.0000021432.70309.28.
27. **Gong H, Rehman J, Tang H, Wary K, Mittal M, Chaturvedi P, Zhao YY, Komarova YA, Vogel SM, Malik AB.** HIF2α signaling inhibits adherens junctional disruption in acute lung injury. *J Clin Invest* 125: 652–664, 2015. doi:10.1172/JCI77701.
28. **Good RB, Gilbane AJ, Trinder SL, Denton CP, Coghlan G, Abraham DJ, Holmes AM.** Endothelial to mesenchymal transition contributes to endothelial dysfunction in pulmonary arterial hypertension. *Am J Pathol* 185: 1850–1858, 2015. doi:10.1016/j.ajpath.2015.03.019.
29. **Hickey MM, Richardson T, Wang T, Mosqueira M, Arguiri E, Yu H, Yu QC, Solomides CC, Morrisey EE, Khurana TS, Christofidou-Solomidou M, Simon MC.** The von Hippel-Lindau Chuvash mutation promotes pulmonary hypertension and fibrosis in mice. *J Clin Invest* 120: 827–839, 2010. doi:10.1172/JCI36362.
30. **Hopper RK, Moonen JR, Diebold I, Cao A, Rhodes CJ, Tojais NF, Hennigs JK, Gu M, Wang L, Rabinovitch M.** In pulmonary arterial hypertension, reduced BMPR2 promotes endothelial-to-mesenchymal transition via HMGA1 and its target Slug. *Circulation* 133: 1783–1794, 2016. doi:10.1161/CIRCULATIONAHA.115.020617.
31. **Howard LS, Crosby A, Vaughan P, Sobolewski A, Southwood M, Foster ML, Chilvers ER, Morrell NW.** Distinct responses to hypoxia in subpopulations of distal pulmonary artery cells contribute to pulmonary vascular remodeling in emphysema. *Pulm Circ* 2: 241–249, 2012. doi:10.4103/2045-8932.97616.
32. **Hu CJ, Wang LY, Chodosh LA, Keith B, Simon MC.** Differential roles of hypoxia-inducible factor 1α (HIF-1α) and HIF-2α in hypoxic gene regulation. *Mol Cell Biol* 23: 9361–9374, 2003. doi:10.1128/MCB.23.24.9361-9374.2003.
33. **Humbert M, Morrell NW, Archer SL, Stenmark KR, MacLean MR, Lang IM, Christman BW, Weir EK, Eickelberg O, Voelkel NF, Rabinovitch M.** Cellular and molecular pathobiology of pulmonary arterial hypertension. *J Am Coll Cardiol* 43, *Suppl S*: 13S–24S, 2004. doi:10.1016/j.jacc.2004.02.029.
34. **Ivan M, Kondo K, Yang H, Kim W, Valiando J, Ohh M, Salic A, Asara JM, Lane WS, Kaelin WG Jr.** HIFα targeted for VHL-mediated destruction by proline hydroxylation: implications for O_2 sensing. *Science* 292: 464–468, 2001. doi:10.1126/science.1059817.
35. **Jaakkola P, Mole DR, Tian YM, Wilson MI, Gielbert J, Gaskell SJ, von Kriegsheim A, Hebestreit HF, Mukherji M, Schofield CJ, Maxwell PH, Pugh CW, Ratcliffe PJ.** Targeting of HIF-α to the von Hippel-Lindau ubiquitylation complex by O_2-regulated prolyl hydroxylation. *Science* 292: 468–472, 2001. doi:10.1126/science.1059796.
36. **Kapitsinou PP, Rajendran G, Astleford L, Michael M, Schonfeld MP, Fields T, Shay S, French JL, West J, Haase VH.** The endothelial prolyl-4-hydroxylase domain 2/hypoxia-inducible factor 2 axis regulates pulmonary artery pressure in mice. *Mol Cell Biol* 36: 1584–1594, 2016. doi:10.1128/MCB.01055-15.
37. **Kisanuki YY, Hammer RE, Miyazaki J, Williams SC, Richardson JA, Yanagisawa M.** Tie2-Cre transgenic mice: a new model for endothelial cell-lineage analysis in vivo. *Dev Biol* 230: 230–242, 2001. doi:10.1006/dbio.2000.0106.
38. **Kokudo T, Suzuki Y, Yoshimatsu Y, Yamazaki T, Watabe T, Miyazono K.** Snail is required for TGFβ-induced endothelial-mesenchymal transition of embryonic stem cell-derived endothelial cells. *J Cell Sci* 121: 3317–3324, 2008. doi:10.1242/jcs.028282.
39. **Kovacic JC, Mercader N, Torres M, Boehm M, Fuster V.** Epithelial-to-mesenchymal and endothelial-to-mesenchymal transition: from cardiovascular development to disease. *Circulation* 125: 1795–1808, 2012. doi:10.1161/CIRCULATIONAHA.111.040352.
40. **Lee G, Won H-S, Lee Y-M, Choi J-W, Oh T-I, Jang J-H, Choi D-K, Lim B-O, Kim YJ, Park J-W, Puigserver P, Lim J-H.** Oxidative dimerization of PHD2 is responsible for its inactivation and contributes to metabolic reprogramming via HIF-1α activation. *Sci Rep* 6: 18928, 2016. doi:10.1038/srep18928.
41. **Lei Y, Hu T, Wu X, Wu Y, Bao Q, Zhang L, Xia H, Sun H, You Q, Zhang X.** Affinity-based fluorescence polarization assay for high-throughput screening of prolyl hydroxylase 2 inhibitors. *ACS Med Chem Lett* 6: 1236–1240, 2015. doi:10.1021/acsmedchemlett.5b00394.
42. **Leopold JA, Maron BA.** Molecular mechanisms of pulmonary vascular remodeling in pulmonary arterial hypertension. *Int J Mol Sci* 17: E761, 2016. doi:10.3390/ijms17050761.
43. **Li ZH, Bresnick AR.** The S100A4 metastasis factor regulates cellular motility via a direct interaction with myosin-IIA. *Cancer Res* 66: 5173–5180, 2006. doi:10.1158/0008-5472.CAN-05-3087.
44. **Liang S, Yu H, Chen X, Shen T, Cui Z, Si G, Zhang J, Cheng Y, Jia S, Song S, Zhang X, Yu X.** PDGF-BB/KLF4/VEGF signaling axis in pulmonary artery endothelial cell angiogenesis. *Cell Physiol Biochem*: 41: 2333–2349, 2017. doi:10.1159/000475652.
45. **Liu S, Kumar SM, Martin JS, Yang R, Xu X.** Snail1 mediates hypoxia-induced melanoma progression. *Am J Pathol* 179: 3020–3031, 2011. doi:10.1016/j.ajpath.2011.08.038.
46. **Liu Y, Zou J, Li B, Wang Y, Wang D, Hao Y, Ke X, Li X.** RUNX3 modulates hypoxia-induced endothelial-to-mesenchymal transition of human cardiac microvascular endothelial cells. *Int J Mol Med* 40: 65–74, 2017. doi:10.3892/ijmm.2017.2998.
47. **Long L, Crosby A, Yang X, Southwood M, Upton PD, Kim DK, Morrell NW.** Altered bone morphogenetic protein and transforming growth factor-β signaling in rat models of pulmonary hypertension: potential for activin receptor-like kinase-5 inhibition in prevention and progression of disease. *Circulation* 119: 566–576, 2009. doi:10.1161/CIRCULATIONAHA.108.821504.
48. **Lu H, Chen I, Shimoda LA, Park Y, Zhang C, Tran L, Zhang H, Semenza GL.** Chemotherapy-induced Ca^{2+} release stimulates breast cancer stem cell enrichment. *Cell Reports* 18: 1946–1957, 2017. doi:10.1016/j.celrep.2017.02.001.
49. **Ma Z, Zhu L, Liu Y, Wang Z, Yang Y, Chen L, Lu Q.** Lovastatin alleviates endothelial-to-mesenchymal transition in glomeruli via suppression of oxidative stress and TGF-β1 signaling. *Front Pharmacol* 8: 473, 2017. doi:10.3389/fphar.2017.00473.
50. **Maarman G, Lecour S, Butrous G, Thienemann F, Sliwa K.** A comprehensive review: the evolution of animal models in pulmonary

Downloaded from journals.physiology.org/journal/ajplung at Midwestern Univ Lib (132.174.254.157) on December 20, 2022.

hypertension research; are we there yet? *Pulm Circ* 3: 739–756, 2013. doi:10.1086/674770.

51. **McMahon S, Charbonneau M, Grandmont S, Richard DE, Dubois CM.** Transforming growth factor β1 induces hypoxia-inducible factor-1 stabilization through selective inhibition of PHD2 expression. *J Biol Chem* 281: 24171–24181, 2006. doi:10.1074/jbc.M604507200.
52. **Minamishima YA, Moslehi J, Bardeesy N, Cullen D, Bronson RT, Kaelin WG Jr.** Somatic inactivation of the PHD2 prolyl hydroxylase causes polycythemia and congestive heart failure. *Blood* 111: 3236–3244, 2008. doi:10.1182/blood-2007-10-117812.
53. **Mole DR, Blancher C, Copley RR, Pollard PJ, Gleadle JM, Ragoussis J, Ratcliffe PJ.** Genome-wide association of hypoxia-inducible factor (HIF)-1α and HIF-2α DNA binding with expression profiling of hypoxia-inducible transcripts. *J Biol Chem* 284: 16767–16775, 2009. doi:10.1074/jbc.M901790200.
54. **Nie L, Lyros O, Medda R, Jovanovic N, Schmidt JL, Otterson MF, Johnson CP, Behmaram B, Shaker R, Rafiee P.** Endothelial-mesenchymal transition in normal human esophageal endothelial cells cocultured with esophageal adenocarcinoma cells: role of IL-1β and TGF-β2. *Am J Physiol Cell Physiol* 307: C859–C877, 2014. doi:10.1152/ajpcell.00081.2014.
55. **Nikitopoulou I, Orfanos SE, Kotanidou A, Maltabe V, Manitsopoulos N, Karras P, Kouklis P, Armaganidis A, Maniatis NA.** Vascular endothelial-cadherin downregulation as a feature of endothelial transdifferentiation in monocrotaline-induced pulmonary hypertension. *Am J Physiol Lung Cell Mol Physiol* 311: L352–L363, 2016. doi:10.1152/ajplung.00156.2014.
56. **Osorio LA, Farfán NM, Castellón EA, Contreras HR.** SNAIL transcription factor increases the motility and invasive capacity of prostate cancer cells. *Mol Med Rep* 13: 778–786, 2016. doi:10.3892/mmr.2015.4585.
57. **Peng YJ, Nanduri J, Khan SA, Yuan G, Wang N, Kinsman B, Vaddi DR, Kumar GK, Garcia JA, Semenza GL, Prabhakar NR.** Hypoxia-inducible factor 2α (HIF-2α) heterozygous-null mice exhibit exaggerated carotid body sensitivity to hypoxia, breathing instability, and hypertension. *Proc Natl Acad Sci USA* 108: 3065–3070, 2011. doi:10.1073/pnas.1100064108.
58. **Pérot G, Derré J, Coindre JM, Tirode F, Lucchesi C, Mariani O, Gibault L, Guillou L, Terrier P, Aurias A.** Strong smooth muscle differentiation is dependent on myocardin gene amplification in most human retroperitoneal leiomyosarcomas. *Cancer Res* 69: 2269–2278, 2009. doi:10.1158/0008-5472.CAN-08-1443.
59. **Pietra GG, Edwards WD, Kay JM, Rich S, Kernis J, Schloo B, Ayres SM, Bergofsky EH, Brundage BH, Detre KM.** Histopathology of primary pulmonary hypertension. A qualitative and quantitative study of pulmonary blood vessels from 58 patients in the National Heart, Lung, and Blood Institute, Primary Pulmonary Hypertension Registry. *Circulation* 80: 1198–1206, 1989. doi:10.1161/01.CIR.80.5.1198.
60. **Ranchoux B, Antigny F, Rucker-Martin C, Hautefort A, Péchoux C, Bogaard HJ, Dorfmüller P, Remy S, Lecerf F, Planté S, Chat S, Fadel E, Houssaini A, Anegon I, Adnot S, Simonneau G, Humbert M, Cohen-Kaminsky S, Perros F.** Endothelial-to-mesenchymal transition in pulmonary hypertension. *Circulation* 131: 1006–1018, 2015. doi:10.1161/CIRCULATIONAHA.114.008750.
61. **Reynolds AM, Holmes MD, Danilov SM, Reynolds PN.** Targeted gene delivery of BMPR2 attenuates pulmonary hypertension. *Eur Respir J* 39: 329–343, 2012. doi:10.1183/09031936.00187310.
62. **Rieder F, Kessler SP, West GA, Bhilocha S, de la Motte C, Sadler TM, Gopalan B, Stylianou E, Fiocchi C.** Inflammation-induced endothelial-to-mesenchymal transition: a novel mechanism of intestinal fibrosis. *Am J Pathol* 179: 2660–2673, 2011. doi:10.1016/j.ajpath.2011.07.042.
63. **Sakao S, Tatsumi K, Voelkel NF.** Endothelial cells and pulmonary arterial hypertension: apoptosis, proliferation, interaction and transdifferentiation. *Respir Res* 10: 95, 2009. doi:10.1186/1465-9921-10-95.
64. **Semenza GL.** Oxygen sensing, hypoxia-inducible factors, and disease pathophysiology. *Annu Rev Pathol* 9: 47–71, 2014. doi:10.1146/annurev-pathol-012513-104720.
65. **Shimoda LA, Laurie SS.** HIF and pulmonary vascular responses to hypoxia. *J Appl Physiol (1985)* 116: 867–874, 2014. doi:10.1152/japplphysiol.00643.2013.
66. **Shimoda LA, Semenza GL.** HIF and the lung: role of hypoxia-inducible factors in pulmonary development and disease. *Am J Respir Crit Care Med* 183: 152–156, 2011. doi:10.1164/rccm.201009-1393PP.
67. **Sperber H, Mathieu J, Wang Y, Ferreccio A, Hesson J, Xu Z, Fischer KA, Devi A, Detraux D, Gu H, Battle SL, Showalter M, Valensisi C, Bielas JH, Ericson NG, Margaretha L, Robitaille AM, Margineantu D, Fiehn O, Hockenbery D, Blau CA, Raftery D, Margolin AA, Hawkins RD, Moon RT, Ware CB, Ruohola-Baker H.** The metabolome regulates the epigenetic landscape during naive-to-primed human embryonic stem cell transition. *Nat Cell Biol* 17: 1523–1535, 2015. doi:10.1038/ncb3264.
68. **Stahnke T, Kowtharapu BS, Stachs O, Schmitz KP, Wurm J, Wree A, Guthoff RF, Hovakimyan M.** Suppression of TGF-β pathway by pirfenidone decreases extracellular matrix deposition in ocular fibroblasts in vitro. *PLoS One* 12: e0172592, 2017. doi:10.1371/journal.pone.0172592.
69. **Stenmark KR, Meyrick B, Galie N, Mooi WJ, McMurtry IF.** Animal models of pulmonary arterial hypertension: the hope for etiological discovery and pharmacological cure. *Am J Physiol Lung Cell Mol Physiol* 297: L1013–L1032, 2009. doi:10.1152/ajplung.00217.2009.
70. **Sutendra G, Dromparis P, Wright P, Bonnet S, Haromy A, Hao Z, McMurtry MS, Michalak M, Vance JE, Sessa WC, Michelakis ED.** The role of Nogo and the mitochondria-endoplasmic reticulum unit in pulmonary hypertension. *Sci Transl Med* 3: 88ra55, 2011. doi:10.1126/scitranslmed.3002194.
71. **Takeda K, Cowan A, Fong GH.** Essential role for prolyl hydroxylase domain protein 2 in oxygen homeostasis of the adult vascular system. *Circulation* 116: 774–781, 2007. doi:10.1161/CIRCULATIONAHA.107.701516.
72. **Tang H, Chen J, Fraidenburg DR, Song S, Sysol JR, Drennan AR, Offermanns S, Ye RD, Bonini MG, Minshall RD, Garcia JG, Machado RF, Makino A, Yuan JX.** Deficiency of Akt1, but not Akt2, attenuates the development of pulmonary hypertension. *Am J Physiol Lung Cell Mol Physiol* 308: L208–L220, 2015. doi:10.1152/ajplung.00242.2014.
73. **Tang H, Yamamura A, Yamamura H, Song S, Fraidenburg DR, Chen J, Gu Y, Pohl NM, Zhou T, Jiménez-Pérez L, Ayon RJ, Desai AA, Goltzman D, Rischard F, Khalpey Z, Black SM, Garcia JG, Makino A, Yuan JX.** Pathogenic role of calcium-sensing receptors in the development and progression of pulmonary hypertension. *Am J Physiol Lung Cell Mol Physiol* 310: L846–L859, 2016. doi:10.1152/ajplung.00050.2016.
74. **Thompson O, Moghraby JS, Ayscough KR, Winder SJ.** Depletion of the actin bundling protein SM22/transgelin increases actin dynamics and enhances the tumourigenic phenotypes of cells. *BMC Cell Biol* 13: 1, 2012. doi:10.1186/1471-2121-13-1.
75. **Tian H, McKnight SL, Russell DW.** Endothelial PAS domain protein 1 (EPAS1), a transcription factor selectively expressed in endothelial cells. *Genes Dev* 11: 72–82, 1997. doi:10.1101/gad.11.1.72.
76. **Tuder RM, Chacon M, Alger L, Wang J, Taraseviciene-Stewart L, Kasahara Y, Cool CD, Bishop AE, Geraci M, Semenza GL, Yacoub M, Polak JM, Voelkel NF.** Expression of angiogenesis-related molecules in plexiform lesions in severe pulmonary hypertension: evidence for a process of disordered angiogenesis. *J Pathol* 195: 367–374, 2001. doi:10.1002/path.953.
77. **Wang S, Zeng H, Chen ST, Zhou L, Xie XJ, He X, Tao YK, Tuo QH, Deng C, Liao DF, Chen JX.** Ablation of endothelial prolyl hydroxylase domain protein-2 promotes renal vascular remodelling and fibrosis in mice. *J Cell Mol Med* 21: 1967–1978, 2017. doi:10.1111/jcmm.13117.
78. **Wang S, Zeng H, Xie XJ, Tao YK, He X, Roman RJ, Aschner JL, Chen JX.** Loss of prolyl hydroxylase domain protein 2 in vascular endothelium increases pericyte coverage and promotes pulmonary arterial remodeling. *Oncotarget* 7: 58848–58861, 2016. doi:10.18632/oncotarget.11585.
79. **Xiao Y, Peng H, Hong C, Chen Z, Deng X, Wang A, Yang F, Yang L, Chen C, Qin X.** PDGF promotes the Warburg effect in pulmonary arterial smooth muscle cells via activation of the PI3K/AKT/mTOR/HIF-1α signaling pathway. *Cell Physiol Biochem* 42: 1603–1613, 2017. doi:10.1159/000479401.
80. **Xu X, Tan X, Hulshoff MS, Wilhelmi T, Zeisberg M, Zeisberg EM.** Hypoxia-induced endothelial-mesenchymal transition is associated with RASAL1 promoter hypermethylation in human coronary endothelial cells. *FEBS Lett* 590: 1222–1233, 2016. doi:10.1002/1873-3468.12158.
81. **Xu X, Tan X, Tampe B, Sanchez E, Zeisberg M, Zeisberg EM.** Snail is a direct target of hypoxia-inducible factor 1α (HIF1α) in hypoxia-induced endothelial to mesenchymal transition of human coronary endothelial cells. *J Biol Chem* 290: 16653–16664, 2015. doi:10.1074/jbc.M115.636944.

Downloaded from journals.physiology.org/journal/ajplung at Midwestern Univ Lib (132.174.254.157) on December 20, 2022.

83. **Yi ES, Kim H, Ahn H, Strother J, Morris T, Masliah E, Hansen LA, Park K, Friedman PJ.** Distribution of obstructive intimal lesions and their cellular phenotypes in chronic pulmonary hypertension. A morphometric and immunohistochemical study. *Am J Respir Crit Care Med* 162: 1577–1586, 2000. doi:10.1164/ajrccm.162.4.9912131.
84. **Yoo HY, Zeifman A, Ko EA, Smith KA, Chen J, Machado RF, Zhao YY, Minshall RD, Yuan JX.** Optimization of isolated perfused/ventilated mouse lung to study hypoxic pulmonary vasoconstriction. *Pulm Circ* 3: 396–405, 2013. doi:10.4103/2045-8932.114776.
85. **Yuan G, Peng YJ, Reddy VD, Makarenko VV, Nanduri J, Khan SA, Garcia JA, Kumar GK, Semenza GL, Prabhakar NR.** Mutual antagonism between hypoxia-inducible factors 1α and 2α regulates oxygen sensing and cardio-respiratory homeostasis. *Proc Natl Acad Sci USA* 110: E1788–E1796, 2013. doi:10.1073/pnas.1305961110.
86. **Zander MA, Burns SE, Yang G, Kaplan DR, Miller FD.** Snail coordinately regulates downstream pathways to control multiple aspects of mammalian neural precursor development. *J Neurosci* 34: 5164–5175, 2014. doi:10.1523/JNEUROSCI.0370-14.2014.
87. **Zhang P, Wei Y, Wang L, Debeb BG, Yuan Y, Zhang J, Yuan J, Wang M, Chen D, Sun Y, Woodward WA, Liu Y, Dean DC, Liang H, Hu Y, Ang KK, Hung M-C, Chen J, Ma L.** ATM-mediated stabilization of ZEB1 promotes DNA damage response and radioresistance through CHK1. *Nat Cell Biol* 16: 864–875, 2014. doi:10.1038/ncb3013.

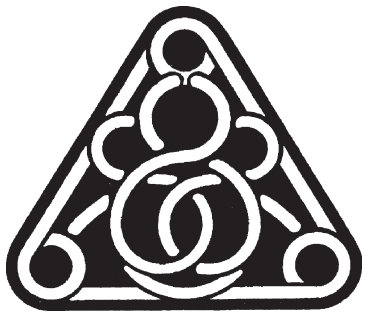

Downloaded from journals.physiology.org/journal/ajplung at Midwestern Univ Lib (132.174.254.157) on December 20, 2022.